

This manuscript is a preprint which is currently under review at the *Journal of Hydrology*. This document has not yet undergone peer review. If accepted, the final version of this manuscript will be available via the 'Peer-reviewed Publication DOI' link on the right-hand side of this webpage. The authors welcome any questions or feedback on this work.

# Saturation excess overland flow accelerates the spread of a generalist soil-borne pathogen

Jean V. Wilkening<sup>a\*</sup>, Enrique Cardillo<sup>b</sup>, Enrique Abad<sup>c</sup>, & Sally E. Thompson<sup>a,d</sup>

<sup>a</sup> Department of Civil and Environmental Engineering, University of California, Berkeley, Berkeley, CA, 94720

<sup>b</sup> Centro de Investigaciones Científicas y Tecnológicas de Extremadura, Mérida, Badajoz 06800, Spain

<sup>c</sup> Departamento de Física Aplicada, Centro Universitario de Mérida and Institute de Computación Científica Avanzada (ICCAEx), Universidad de Extremadura, Badajoz 06800, Mérida, Spain

<sup>d</sup> Department of Civil, Environmental, and Mining Engineering, University of Western Australia, Perth, Western Australia 6009 Australia

\* Corresponding author: jvwilkening@berkeley.edu

## Abstract

Plant pathogens are a major agent of disturbance in ecosystems worldwide. Disturbance by disease can alter the hydrological function of affected ecosystems. However, many plant pathogens are also sensitive to soil moisture and can be propagated by the transport of infectious tissue or reproductive structures in surface flow, so that hydrological processes can drive pathogen infection. These feed-forward and feed-back processes set up the possibility of complex ecohydrological dynamics relating plant disease and the water cycle. Here the generalist root pathogen *Phytophthora cinnamomi* (Pc) is used as a case study to quantify the potential importance of hydrological dynamics on disease spread. A numerical model of Pc growth and dispersal is used to investigate the importance of Pc transport in intermittent surface runoff compared to more continuous rhizosphere Pc spread via diffusion-like hyphal growth. We apply and test this model at two well-studied sites of Pc infection with contrasting hydrology: a *Banksia* woodland in Western Australia where deep sandy soils inhibit surface runoff, and an *Erica* heathland in the Spanish Central Plateau where relatively shallow soils on steep slopes generate intermittent overland flow. Predictions of Pc spatial spread at the Spanish site improve when Pc transport in runoff is incorporated into the model, while no such improvements arise at the Australian site. Omitting transport in overland flow from model predictions at the Spanish site results in an average under-prediction of final pathogen patch areas by 350 m<sup>2</sup> for each year of growth between observations,

highlighting the importance of surface hydrological transport to Pc growth and spread. Hydrological theories that predict the occurrence of overland flow based on soil, topographic, and climate properties can be used to better incorporate this transport pathway and the influence of local hydrological processes in existing Pc risk assessment methods.

**Keywords:** *Phytophthora cinnamomi*, plant pathogens, overland runoff, spatial model

## 1 Introduction

Plant pathogens can affect forest composition, structure, and function, but the dynamics of these disturbances are generally less well understood than compared to those of abiotic disturbances (Flower et al., 2015). Vegetation infection and mortality caused by pathogens can alter forest water balance (Batini et al., 1980; Schofield et al., 1989, e.g.), and there are also potential feed-forward mechanisms by which hydrology can directly impact pathogens. For example, the growth and spread rates of many soil pathogens vary with water potential (Crist et al., 1975; Ferrin et al., 2006; Colhoun, 1973; Malajczuk et al., 1979; Dickenson et al., 1981; Madar et al., 1989; Cook et al., 1972; Boyer, 1995; Schober et al., 1999; Suleman et al., 2001; Desprez-Loustau et al., 2006), meaning that pathogen infection can influence, while also being influenced by, root zone water dynamics. The potential for pathogen propagules and infectious material to be transported by surface flow adds scope for further complex hydrological - pathogen feedback processes. In previous work, relationships between soil water potential and pathogen dynamics were used to relate regional hydroclimatic variations to pathogen risk (Thompson et al., 2013; Thompson et al., 2014). The influence of hydrological transport processes on more localized pathogen spread, however, remain largely unexplored. Yet better understanding of this feed-forward relationship between hydrology and disease disturbance is necessary for understanding coupled forest - pathogen - water systems and the implications for disturbance and ecosystem function.

In this study, we consider the soil-borne pathogen *Phytophthora cinnamomi* (Pc) as a case study of hydrological transport mechanisms for disease spread. Pc is one of the world's most destructive plant pathogens (Burgess et al., 2017), posing a global threat to natural and agricultural systems (Lowe et al., 2000) that is expected to worsen as climates warm (Thompson et al., 2014; Chakraborty et al., 2000; Bergot et al., 2004). Pc forms necrotic lesions on roots and stems of infected host plants. Severe infection results in the loss of the majority of the fine root system in susceptible plants, inhibiting water uptake and causing mortality. Pc is a generalist pathogen affecting a huge array of plant species. For example, in south-west Western Australia, some 40% of the more than 5000 endemic plant species are susceptible to Pc (Shearer, CE Crane, et al., 2004). In Europe, Pc is decimating oak woodlands of *Quercus ilex* and *Quercus suber* (Brasier, 1996) and the chestnut forests (Vettraino et al., 2005). Pc is persistent in the environment and spreads rapidly through infected soil and water. Within the soil, it can spread

via mycelial growth and root-root contact, and through the production of oospores, or motile zoocytes (Hardham et al., 2018). Under unfavorable conditions such as drought, Pc forms resilient chlamydospores that can persist and remain viable for months to years (Jung, Colquhoun, et al., 2013; Hwang et al., 1978). Long-distance spread occurs through the mobilization of infected roots, soil, or fungal propagules by natural and anthropogenic processes (Ristaino et al., 2000).

In natural ecosystems, management strategies to address Pc infection involve prioritizing areas for quarantine, monitoring, and treatment. A component of this prioritization involves making assessments about the likely pathways and rates of Pc establishment and spread in a given landscape (e.g. National Heritage Trust and Environment Australia, 2001; Commonwealth of Australia, 2014). Quantitative modeling provides an avenue to predict the importance of these pathways in a given setting. The growth dynamics of Pc are strongly coupled to environmental conditions (Thompson et al., 2013). Mycelial growth is inhibited under low water potentials (i.e. dry soil), declines with falling temperatures (Malajczuk et al., 1979), and the pathogen is killed by protracted sub-freezing conditions (Marçais et al., 1996). In previous work, we used these environmental dependencies to predict the likelihood of Pc infection across soil type and climate conditions under steady state conditions (Thompson et al., 2013; Thompson et al., 2014). Here, we extend the modeling framework to consider the spatial dynamics of Pc spread and its dependence on transport processes in the environment, with a particular focus on how varying local hydrology impacts these processes.

We address the following research questions:

- Can the rate of Pc spread from disease foci within susceptible plant communities be predicted as a function of soil, plant and climate properties?, and
- How do different mechanisms of pathogen mobility contribute to observed patterns of Pc infection spread?

We consider multiple potential transport pathways that could contribute to Pc spread around disease foci. Mycelial root pathogens, including Pc, spread locally via growth along the host root system, a process that is well-represented via diffusion in soil pathogen models (Cunniffe et al., 2008; Park et al., 2001). Pc also spreads locally due to zoocyte motility. In practice, the maximum observed scales of zoocyte movement and of mycelial extension are comparable, on the order of millimeters per day (Benjamin et al., 1982; Malajczuk et al., 1979). Since observations of disease patches are typically coarse in space and time (e.g. observed on monthly timescales or longer, and on spatial scales of one to tens of meters) (Dawson et al., 1985; Cardillo et al., 2018; Wilson et al., 2012), it is unlikely that the relative contribution of motile zoocytes versus mycelial expansion to this local growth can be determined, and thus will be considered jointly represented by the “diffusive” spread. However, natural (rather than anthropogenic) transport of Pc may not be limited to the rhizosphere. Observations of Pc

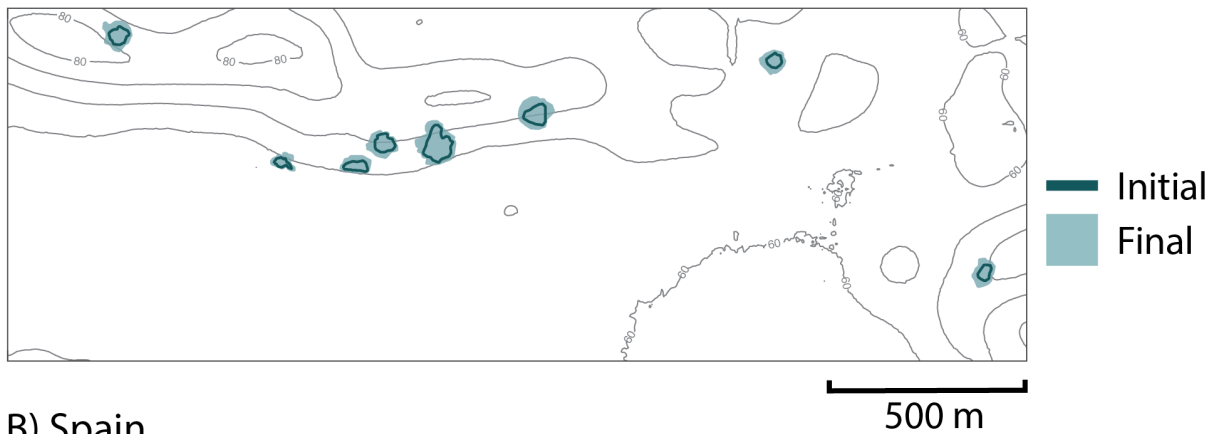
spread persistently reveal features - such as faster downslope than upslope spread, or spatial associations between Pc infection and surface flow channels - which are consistent with Pc transport in surface flow (see Table 1 for details). Although repeated recovery of Pc material in surface flow, subsurface flows and drainage waters (Thomson et al., 1974; Kliejunas et al., 1976; Kinal et al., 1993; Reeser et al., 2011) supports the feasibility of this transport mechanism, its importance is not well understood. Pc will not grow in permanently saturated conditions (Malajczuk et al., 1979), but water flow outside such areas tends to be episodic and infrequent - associated with intense storms (Horton, 1933) or transient saturation of soils (Dunne et al., 1970). Although the intermittent nature of surface runoff might suggest it is unimportant for Pc spread, water could readily transport Pc over tens to hundreds of meters, suggesting that its role should be explored.

Table 1: Evidence of transport of *Pc* via surface water

Study	Location	Species	Observation
G. M. Weste et al. (1971)	Victoria, Australia	<i>P. cinnamomi</i>	Pathogen associated with presence of drainage channels
Podger (1972)	Western Australia	<i>P. cinnamomi</i>	Disease more frequent and faster spreading along drainage lines
G. Weste and Law (1973)	Victoria, Australia	<i>P. cinnamomi</i>	Rapid downhill expansion (up to 400 m/yr), particularly during wet summer
Thomson et al. (1974)	Arizona, USA	Various Phytophthora species	Found Phytophthora propagules in recycled irrigation water from citrus crops
G. Weste, Ruppin, et al. (1976)	Victoria, Australia	<i>P. cinnamomi</i>	Disease spread with clearly defined boundaries in direction of drainage from road
Kliejunas et al. (1976)	Hawaii, USA	<i>P. cinnamomi</i>	Recovery of zoospores in runoff water
Shea et al. (1983)	Western Australia	<i>P. cinnamomi</i>	Lateral transport of zoospores in subsurface water above lateritic layer
Kinal et al. (1993)	Western Australia	<i>P. cinnamomi</i>	Recovered pathogen from laterally flowing subsurface water in lateritic soil
Hill et al. (1994)	Western Australia	<i>P. cinnamomi</i>	Faster spreading disease fronts in low-lying areas than compared to upslope areas
Reeser et al. (2011)	Oregon and Alaska, USA	Various Phytophthora species	Recovered Phytophthora from streams in forested areas
Jung and Dobler (2002)	Dominican Republic	<i>P. cinnamomi</i>	Disease spread follows downslope path of runoff from diseased trees
Oudemans (1999)	New Jersey, USA	<i>P. cinnamomi</i>	Recovered pathogen from streams, irrigation reservoirs, and drainage canals

To better understand the drivers of Pc spread at the hillslope scale, we extend the Pc growth model presented in Thompson et al. (2013) and Thompson et al. (2014) to account for spatial spread of Pc. We include diffusion-like local spread and passive transport in surface water. The model is calibrated and tested at two contrasting sites in Western Australia and Spain. The spatial spread of Pc infection at both sites has been intensively monitored, displaying quite different spatial patterns (Figure 1). We calibrate the model twice at each site, including and omitting overland flow as a Pc transport mechanism, and compare the model performance in each case. The degradation in model performance when overland flow is omitted (in the “diffusion optimized setup”) provides a metric of whether including overland flow is *necessary* to describe observed patterns of spread. The fully calibrated models (including the overland flow terms) are then run without overland flow. The resulting predictions of the spatial patterns provide an estimate of the relative importance of “diffusive” dispersal versus transport in surface runoff for disease spread at each site. The model does not include transport in *subsurface* water flows: subsurface lateral flow is negligible above the water table at the Western Australian site (Xu et al., 2003; Salama et al., 2005), and while the saturated hydraulic conductivity of the soils at the Spanish site is reasonably high (4.47 cm/min (Gómez-Paccard et al., 2015)), the soil moisture content of the soils is generally low (see Section H), greatly reducing soil conductivity and limiting lateral transport in unsaturated soils. In general, however, such subsurface transport is feasible and should be considered in sites where significant lateral subsurface flows occur (Shea et al., 1983; Kinal et al., 1993).

### A) Western Australia



### B) Spain

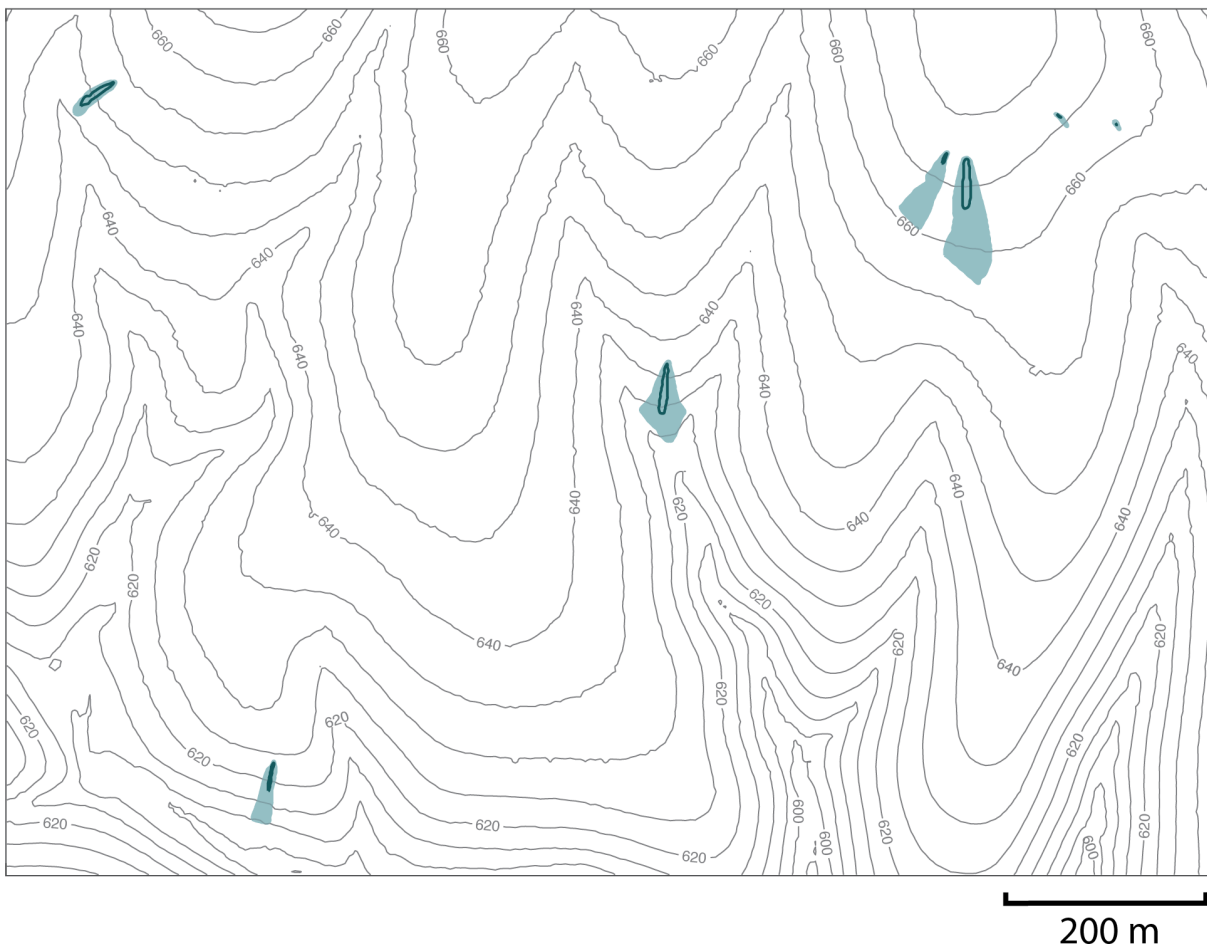


Figure 1: Distinct pathogen spread patterns observed at the site in Western Australia (A) and the site in Spain (B). Topographic contours are shown in 5 meter increments.

## 2 Model

The mean-field spatial dynamics of soil-borne pathogens can be modeled with reaction-diffusion type equations (Park et al., 2001; Cunniffe et al., 2008), specifying the growth rate of pathogen biomass at a point, and its diffusivity (Andow et al., 1990; Okubo et al., 2013). The strong dependence of  $P_c$  mycelial



growth and survival on soil moisture and temperature means that both growth and diffusion terms in the spread model are functions of local environmental conditions. The soil environmental conditions must therefore also be modeled or prescribed based on climate observations and local soil properties. To add transport via overland flow to this model involves specifying a soil water excess available to produce runoff, a routing model to define the direction of flow, and a representation of mobilization, mixing and deposition of propagules in the surface water flow. The model thus has three components: a soil water balance model (detailed in Section 2.1), a runoff routing and propagule transport model (detailed in Section 2.2), and the pathogen growth and spread model (detailed in Section 2.3). The model is implemented on a two-dimensional square grid, where cells take dimensions of  $\Delta x$  and  $\Delta y$ . Table 2 summarizes all the variables and parameters of the model components, and a schematic showing the relation between components is shown in Figure 2.

## 2.1 Soil water balance

Soil water is represented with a mass balance model (Figure 2A) within a homogeneous vertical domain  $z_r$  [mm], taken here as either the depth of the host plants' root zone or the depth to an impermeable soil layer, whichever is smaller. The mean relative soil water content  $s$  [-] in this zone is given by  $s = V_{water}/(nz_r)$ , where  $V_{water}$  is the volume of water per unit area [mm] and  $n$  is the porosity of the soil [-]. The mass balance for the soil moisture is given by:

$$\frac{\partial s}{\partial t} = \frac{f(P(t), s(t), K_{sat}) - g(ET_{max}(t), s(t)) - L(s(t), K_{sat})}{n \times z_r} \quad (1)$$

where  $f()$  represents the rate of infiltration,  $g()$  the rate of evapotranspiration, and  $L()$  the rate of leakage at the bottom boundary. This mass balance is implemented independently for each spatial location. Lateral transport of water in the soil is assumed negligible.

The rate of infiltration is defined as a function of the rainfall rate  $P$  [mm/day], the soil moisture, and the soil infiltration capacity, which we approximate with its saturated hydraulic conductivity  $K_{sat}$  [mm/day], as follows:

$$f(P(t), s(t), K_{sat}) = \begin{cases} P & P < K_{sat} \text{ and } s < 1 \\ K_{sat} & P \geq K_{sat} \text{ and } s < 1 \\ 0 & s = 1 \end{cases} \quad (2)$$

Soil moisture losses via evapotranspiration are described by a piece-wise function of soil moisture, following the approach of Porporato et al. (2004):

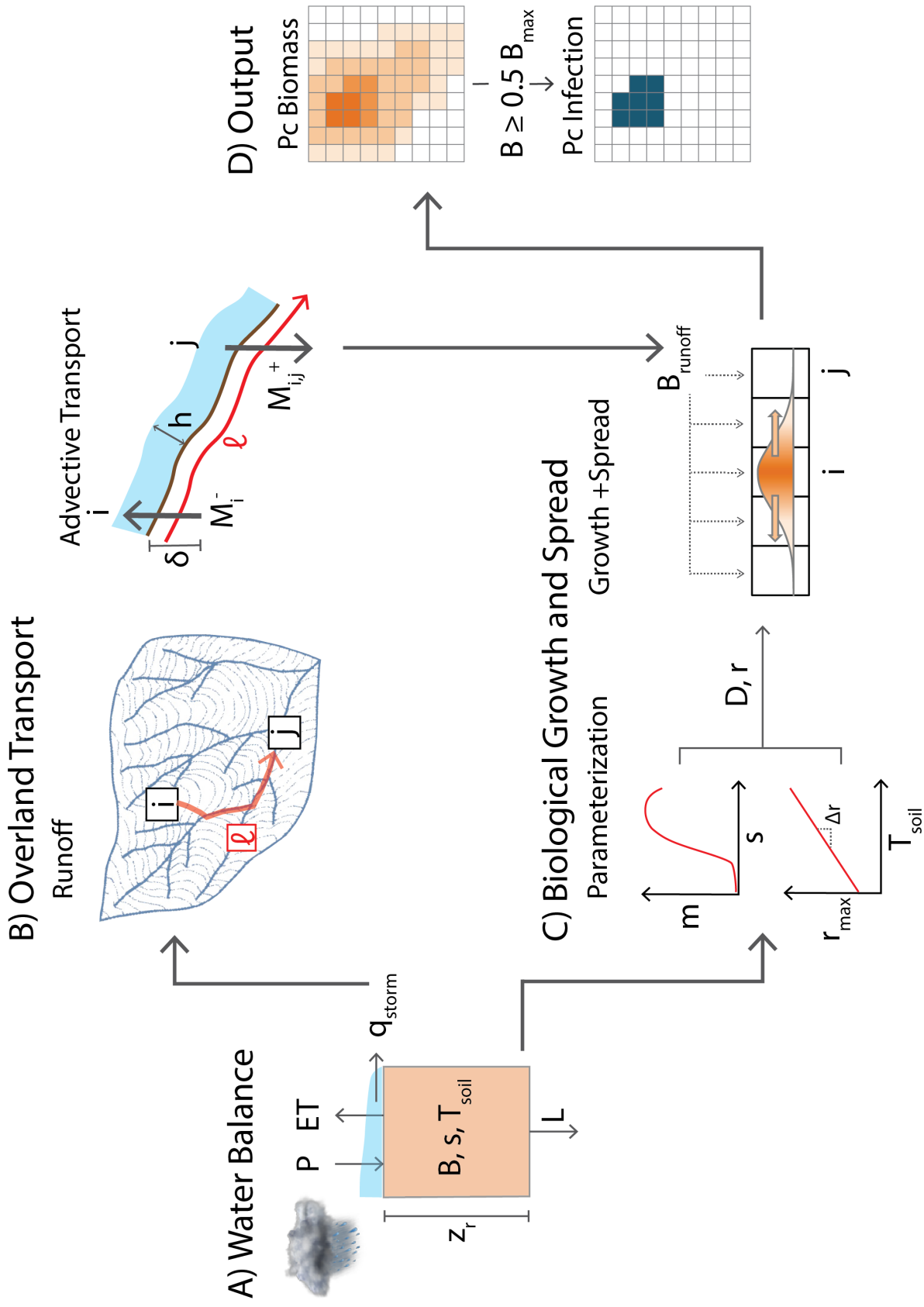


Figure 2: During each time step, the water balance for the soil is computed (A) with precipitation as the input and evapotranspiration (ET), leakage (L), and overland flow ( $q_{storm}$ ) as outputs. In the event of overland flow generation, the routing of runoff between source (i) and sink (j) cells along flowpaths ( $l$ ) and the resulting advective transport is calculated in the overland transport portion of the model (B). The soil moisture and temperature from the water balance and environmental conditions are used to parameterize the growth rate and diffusion coefficient (C) which, along with any input from overland transport, determine the change in biomass density in each cell. With these changes in biomass density, the Pc biomass density field is output at the end of each time step (D). This is then further binarized to presence or absence of Pc infection, where cells with biomass density at least  $0.5B_{max}$  categorized as infected.

$$g(s) = \begin{cases} 0 & s \leq s_{wp} \\ ET_{max} \frac{s-s_{wp}}{s^*-s_{wp}} & s_{wp} < s < s^* \\ ET_{max} & s^* \leq s, \end{cases} \quad (3)$$

where  $s_{wp}$  is the soil moisture wilting point (i.e. plants stop transpiring), and  $s^*$  is the point of complete stomatal opening. Equation 3 states that evaporative losses are negligible below the wilting point, linearly increase with increasing soil moisture between the wilting point and the point of complete stomatal opening, and proceed at a maximum rate  $ET_{max}$  in wetter soils. We make the additional simplifications of: (i) prescribing  $s_{wp}$ ,  $s^*$ , and  $n$  as a function of soil type, (ii) estimating  $ET_{max}$  from weather data (see Section 3.1), and (iii) neglecting any possible relationship between Pc infection, plant health, and evaporation dynamics. Leakage [mm/day] at the bottom boundary to deeper soils follows Porporato et al. (2004):

$$L(s(t), K_{sat}) = K_{sat} s^{2b+3} \quad (4)$$

where  $b$  [-] is the exponent of the soil-water retention curve for the corresponding soil type from Clapp et al. (1978). For cases where the bottom boundary of the modeled soil domain is impervious, the leakage term is set to zero.

The water balance connects to the other two model components via the value of the soil moisture  $s$ , which is used as input to the pathogen biomass growth model (see Section 2.3 and Figure 2C), and by the production of overland flow  $q = P - f$  [mm/day], which is produced when soils are saturated ( $s = 1$ ) or when precipitation occurs a rate exceeding the infiltration capacity of the soil. The runoff model (Figure 2B and Figure 3), described in more detail in Section 2.2, operates on the storm-averaged rate of flow production, ( $q_{storm}$ , mm day<sup>-1</sup>):

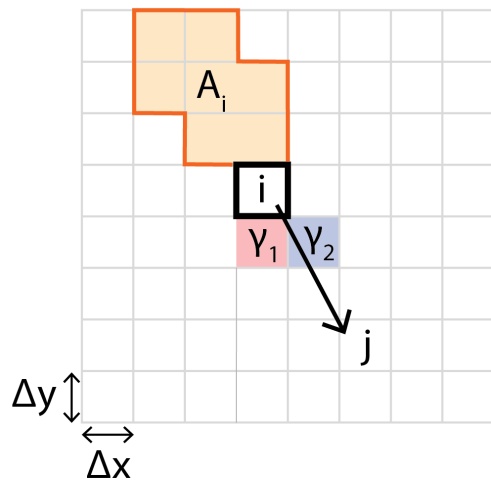
$$q_{storm} = \frac{\sum_{t=0}^{t=t_{storm}} q(t) \Delta t}{t_{storm}} \quad (5)$$

where  $t_{storm}$  [day] is the length of the storm event and  $\Delta t$  is the time step resolution of the model [day]. The duration of a storm event is considered to be the cumulative time of consecutive non-zero precipitation records, up to a maximum of 24 hours, after which it is treated as two discrete events.

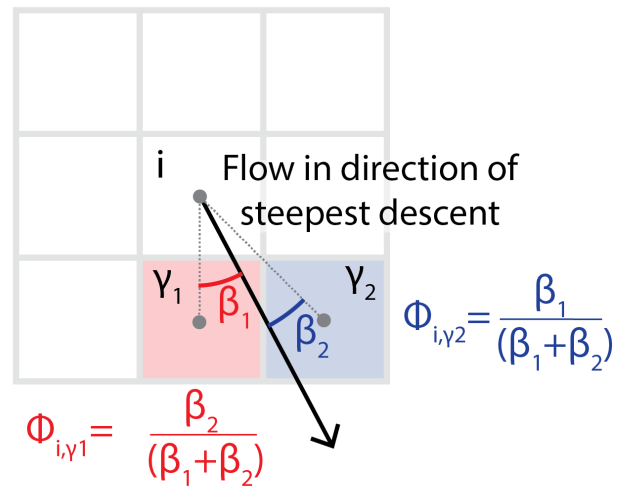
## 2.2 Surface flow routing and propagule transport

This component of the model is new to this study, and therefore explained in detail below. Figure 3 outlines several of the key components of the transport model.

A) Routing on topographic grid



D-∞ algorithm



B) Superposition of concentrations and sink fluxes at Cell j

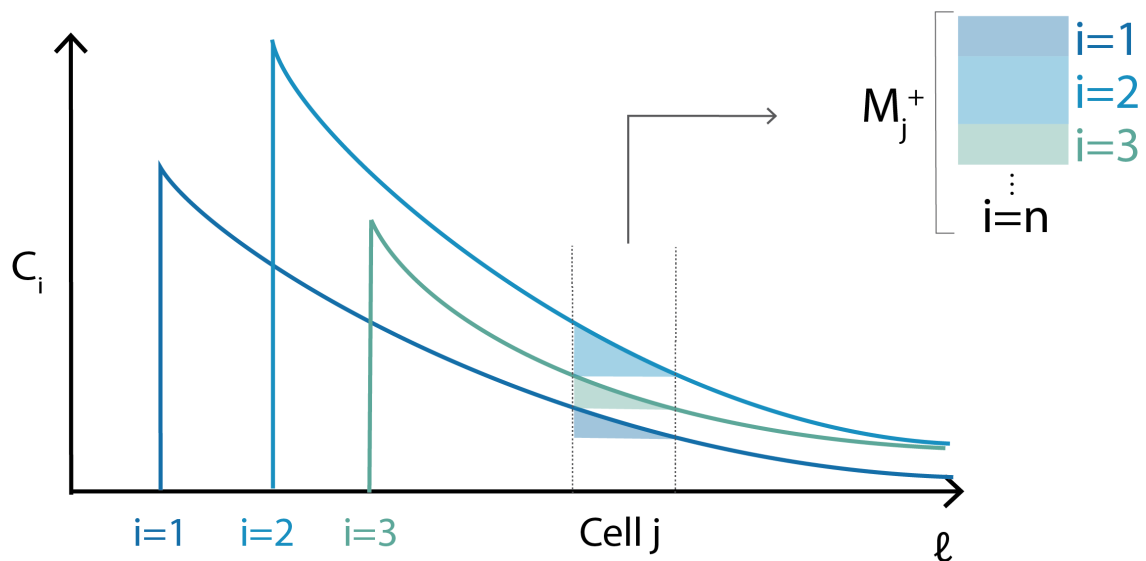


Figure 3: In the flow routing portion of the model (A), the D-∞ algorithm (Tarboton, 1997) is used to determine the flow between a source cell (i) with upslope area  $A_i$  and a downslope sink cell (j). In the algorithm, flow is assumed to travel in the direction of the steepest downhill descent. When this results in flow being split between two adjacent cells, the relative fraction to each cell ( $\phi$ ) is determined by the angles as shown in (A). For each sink cell, the contributions of each upslope source cell are treated individually, with the final cumulative deposited biomass ( $M_j^+$ ) coming from the superposition of all the upslope sources (B).

### 2.2.1 Surface flow routing

Storm averaged runoff ( $q_{storm}$ ) is routed along the land surface using the D- $\infty$  method (Tarboton, 1997) which specifies the fraction ( $\phi_{i,j}$ ) of flow in any upslope location (indexed as  $i$ ) that passes through any specified downslope cell (indexed as  $j$ ) (see Figure 3A). We approximate the dynamic processes of runoff production, routing and their variation throughout a storm with a single, storm-averaged rate of flow production, and steady conditions assumed for runoff depths ( $h$ ), bulk velocity ( $u$ ) and transport properties. With these assumptions,  $\phi_{i,j}$  and the average rate of runoff production ( $q_{storm}$ ) fully specify the runoff routing.

### 2.2.2 Pathogen transport

We model the transport of Pc in the flow using a simple advection equation following the mean water flow path. The flow path is not necessarily aligned with the topographic grid, and has its own coordinate,  $\ell$  [m] (Figure 2B). For flow along this path, the concentration of pathogen biomass ( $C$ , [g m<sup>-3</sup>]) evolves as:

$$\frac{\partial(hC)}{\partial t} = -\frac{\partial q_c C}{\partial \ell} + h(Source - Sink) \quad (6)$$

where  $q_c$  is the water flux per unit width of the flowpath [m<sup>2</sup> day<sup>-1</sup>], and  $Source$  and  $Sink$  denote the rates of concentration increase due to Pc biomass being introduced to the flow from soil beneath the flowpath, and decrease due to its deposition. We assume that deposition follows first order linear kinetics, such that  $Sink(\ell, t) = \beta C(\ell, t)$ , where  $\beta$  [day<sup>-1</sup>] is an unknown rate constant.

With these linear kinetics, and recognizing that the flow is independent of the Pc concentration, we can separately track the fate of biomass concentrations  $C_i$  originating from each upslope source cell  $i$  (Figure 3B). For an individual source cell, the concentration evolves along the downslope flowpath as:

$$\frac{\partial(hC_i)}{\partial t} = -\frac{\partial(q_c C_i)}{\partial \ell} - h\beta C_i \quad (7)$$

Written in this way, the  $Source$  terms in Equation 6 are translated into the boundary conditions on  $C_i$  at location  $i$ . To simplify Equation 7, we apply the steady-state approximation referred to in Section 2.2.1, and approximate the flow depth and velocity along  $\ell$  between cells  $i$  and  $j$ , with their spatial averages  $\bar{h}$  [m] and  $\bar{u}_{i,j}$  [m day<sup>-1</sup>], yielding:

$$0 = -\bar{u}_{i,j} \frac{\partial C_i}{\partial \ell} - \beta C_i \quad (8)$$

This differential equation can be solved to identify the concentration of pathogen biomass in the runoff at location  $j$ , located downstream along the flowpath  $\ell$  from source location  $i$ , that can be attributed to

the mobilization of biomass from source  $i$ :

$$C_i(\ell) = C_{io} e^{\frac{-\beta(\ell_j - \ell_i)}{\bar{u}_{i,j}}} \quad (9)$$

where  $C_{io}$  is the boundary condition for this concentration at cell  $i$  and represents the storm-averaged biomass concentration generated by mobilizing Pc into the flow at that site. The *Sink* term at location  $j$  associated with biomass originating from  $i$  is given by multiplying Equation 9 by the rate constant  $\beta$ , and can be used to compute the total transport of biomass from source location  $i$  to sink location  $j$  during the storm:

$$M_{i,j}^+ = \left( \beta C_{io} e^{\frac{-\beta(\ell_j - \ell_i)}{\bar{u}_{i,j}}} \right) \times \left( \frac{\Delta \ell}{\bar{u}_j} \right) \times (q_{storm} A_i \phi_{i,j} t_{storm}) \quad (10)$$

In this expression,  $A_i$  [m<sup>2</sup>] is the upslope contributing area which generates runoff that passes through cell  $i$ ,  $\bar{u}_j$  [m s<sup>-1</sup>] is the storm-averaged runoff velocity at cell  $j$ , and  $\Delta \ell$  is the travel path length passing through location  $j$  (and can be approximated by the grid size  $\Delta x$ ). Equation 10 can be interpreted as the product of the rate of biomass deposition (first term), the average residence time of water in cell  $j$  (second term), and the total volume of runoff that is routed from  $i$  to  $j$  over the course of the storm (third term).

### 2.2.3 Hydraulic assumptions

To implement Equations 9 and 10, expressions are needed for the distance  $\ell_j - \ell_i$ , as well as the storm-averaged flow velocity and depth terms. We approximate  $\ell_j - \ell_i$  with the Euclidean distance between the points  $i$  and  $j$  ( $\chi_{i,j}$ ). We use Manning's Equation to describe the flow behavior at a point as:

$$u = K h^{\frac{2}{3}} \quad (11)$$

Where  $K$  [m <sup>$\frac{1}{3}$</sup>  day<sup>-1</sup>] is a kinematic resistance factor (Brutsaert et al., 2005), given by  $\sqrt{\text{slope}}/\nu$  where  $\nu$  [day m<sup>- $\frac{1}{3}$</sup> ] parameterizes the resistance of the land surface to flow. For the one dimensional flows we consider, flow velocity  $u = q_c/h$ , and for steady conditions,  $q_c$  depends on the storm averaged rate of runoff production  $q_{storm}$  and the upslope contributing area  $A$ :

$$h = \left( \frac{q_c}{K} \right)^{3/5} = \left( \frac{q_{storm} A}{\Delta y K} \right)^{3/5} \quad (12)$$

where  $\Delta y$  is again used to approximate the flowpath width. With Equation 11, this expression for  $h$  gives the velocity as:

$$u = K \left( \frac{q_{storm} A}{K \Delta y} \right)^{\frac{2}{5}} \quad (13)$$

$u$  can then be used in Equation 10. However, with this substitution, Equation 10 contains two unknown parameters: the linear rate constant  $\beta$ , and the land surface roughness  $\nu$  (forming, with the land surface slope, the kinematic resistance term  $K$ ).

To facilitate calibration of the model, it is helpful to lump these parameters together in a single term within Equation 10, which we express as  $\alpha$ :

$$M_{i,j}^+ = \frac{1}{v_j} \alpha C_{io} e^{\frac{-\alpha x_{i,j}}{v_{i,j}}} \Delta x q_{storm} A_i \phi_{i,j} t_{storm} \quad (14)$$

Where  $\alpha = \nu^{\frac{3}{5}} \beta$ , and  $v$  [ $\text{m}^{\frac{4}{5}} \text{day}^{-\frac{2}{5}}$ ] represents all terms (other than  $\nu$ ) in Equation 13.  $v$  can be defined from topography and storm properties. It is computed at cells  $i$  and  $j$  (giving  $v_i$  and  $v_j$ ) and averaged to give  $v_{i,j}$ , an approximation to its spatial mean along the flow path between the cells.

When Equation 14 is summed over all upslope source cells, it gives the total deposition at a cell  $j$  with  $n$  upslope source cells as a result of an overland runoff event:

$$M_j^+ = \sum_{i=1}^n \frac{1}{v_j} \alpha C_{io} e^{\frac{-\alpha x_{i,j}}{v_{i,j}}} \Delta x q_{storm} A_i \phi_{i,j} t_{storm} \quad (15)$$

#### 2.2.4 Concentration boundary condition due to Pc mobilization at a cell

The only remaining unknown in the transport model is the boundary condition at each source cell  $i$ ,  $C_{io}$ . Source cells are those where Pc biomass areal density  $B_i$  [ $\text{g m}^{-2}$ ] is sufficiently high to cause the host to appear ‘infected’ (see Section 2.4). At these cells, we assume that each runoff generating event will mobilize all Pc biomass within an “effective depth of interaction” ( $\delta$ , mm) (Ahuja et al., 1981), measured downward from the soil surface. This means that there is a specified total biomass  $M_i^-$  [g], that will be transported out from each source cell:

$$M_i^- = \frac{B_i \delta \Delta x \Delta y}{z_r} \quad (16)$$

Mass balance requires that  $M_i^- = \sum_{j=1}^n M_{i,j}^+$  - that is, all biomass originating from  $i$  that is deposited to  $n$  downslope cells must sum to the mobilized biomass from  $i$ . By equating this sum (taken from Equation 15) to the right hand side of Equation 16, it is possible to solve for  $C_{io}$ , providing that all biomass is deposited along the modeled flowpath  $\ell$ . The special case where flowpaths extend outside the model domain is addressed in the Appendix A.

With  $C_{io}$  constrained by the mass balance, Equation 14 can be used to find  $M_{i,j}^+$  for each pair of source-sink cells. Runoff events can result in mobilization of biomass from an infected cell, superposed on deposition of biomass into the same cell from infected cells upslope. The net change in biomass density as a result of overland transport  $B_{runoff}$  [ $\text{g m}^{-2}$ ] is given by combining Equation 15 describing the sink behavior of the cell and Equation 16 describing the source behavior of the cell:

$$B_{runoff} = \frac{M_j^+ - M_i^-}{\Delta x \Delta y} \quad (17)$$

where here the use of both labels  $j$  and  $i$  emphasizes the potentially dual role any site can have as both a source and sink of Pc.

### 2.3 Pathogen growth and diffusive spread

Pathogen biomass density (on a per-area basis,  $B$ , [g/m<sup>2</sup>]) grows following a logistic-type growth equation. The growth rate  $r$  varies with soil moisture  $s$  and temperature ( $T_{soil}$ ), such that  $r = r_{max}(T_{soil}) \times m(s)$ . Here,  $r_{max}(T_{soil})$  represents the growth rate of the mycelia under ambient temperature and optimal soil moisture conditions.  $r_{max}$  varies linearly with temperature as  $r_{max}(T_{soil}) = r_0 + \Delta r T_{soil}$  (Shearer, Shea, et al., 1987), where  $r_0$  is the growth rate in optimal soil moisture conditions at  $T = 0^\circ\text{C}$  and  $\Delta r$  [ $^\circ\text{C}^{-1}$ ] is a fitted parameter describing the temperature dependence of pathogen growth. The function  $m(s)$  represents the effect of changing soil moisture on pathogen growth rates, which are impaired at very high and very low soil water potentials (Malajczuk et al., 1979). From the soil water potentials, we find the relative water content  $s$  using the Brooks-Corey water retention curve (Brooks et al., 1964), and follow Thompson et al. (2013) in approximating  $m(s)$  with a linear piecewise function, shown in Appendix B. We account for a constant (time and environmentally independent) mortality rate for mycelia  $d$  [days<sup>-1</sup>]. The pathogen growth model at a point is given by:

$$\frac{\partial B}{\partial t}_{growth} = [r_{max}(T_{soil})m(s) - d]B \left(1 - \frac{B}{B_{max}}\right), \quad (18)$$

where  $B_{max}$  represents the maximum biomass density that can be sustained at a point, assumed to be constant. Note that the model omits Pc mortality due to freezing (Marçais et al., 1996) as a simplifying measure given the warm temperatures experienced at the case study sites explored here.

### 2.4 Pathogen spread

Pc spread due to the spatial growth of mycelium and dispersal of propagules within the soil is modeled continuously in time and approximated with a diffusive process. The diffusion coefficient is isotropic and is scaled down from its maximum ( $D_{max}$ , m<sup>2</sup>day<sup>-1</sup>) by the soil moisture function  $m(s)$  to ensure that soil moisture conditions that inhibit Pc growth also inhibit Pc spread. Pathogen transport in overland flow appears as the addition of biomass  $B_{runoff}$  (Equation 17), which is non-zero only at the end of a runoff-producing storm event. The biomass model is then given by:

$$\frac{\partial B}{\partial t} = [r_{max}(T_{soil})m(s) - d]B \left(1 - \frac{B}{B_{max}}\right) + D_{max}m(s) \nabla^2 B + B_{runoff} \quad (19)$$



Note that the dynamics of the model are independent of the numerical value of  $B_{max}$ . We define the threshold for host ‘infection’ as  $0.5B_{max}$  (also independently of  $B_{max}$ ), and arbitrarily set  $B_{max}$  to 1 g m<sup>-2</sup>.

Symbol	Description	Dimensions	Units
<b>Discretization</b>			
$\Delta t$	Time step	T	day
$\Delta x, \Delta y$	Spatial step	L	m
<b>Soil moisture balance</b>			
$z_r$	Soil vertical domain	L	mm
$s$	Mean relative soil water content	-	-
$V_{water}$	Volume soil water per unit area	L	mm
$n$	Soil porosity	-	-
$f$	Rate of infiltration	L T <sup>-1</sup>	mm day <sup>-1</sup>
$g$	Rate of evapotranspiration	L T <sup>-1</sup>	mm day <sup>-1</sup>
$K_{sat}$	Soil saturated hydraulic conductivity	L T <sup>-1</sup>	mm day <sup>-1</sup>
$q$	Surface flow rate	L T <sup>-1</sup>	mm day <sup>-1</sup>
$t_{storm}$	Length of storm event	T	day
$s_{wp}$	Soil moisture wilting point	-	-
$s^*$	Soil moisture point of full stomatal opening	-	-
$ET_{max}$	Maximum evapotranspiration rate	L T <sup>-1</sup>	mm day <sup>-1</sup>
$P$	Precipitation rate	L T <sup>-1</sup>	mm day <sup>-1</sup>
$q_{storm}$	Average rate of flow production for storm event	L T <sup>-1</sup>	mm day <sup>-1</sup>
$L$	Rate of leakage at bottom boundary	L T <sup>-1</sup>	mm day <sup>-1</sup>
$b$	Soil-water retention curve exponent	-	-
<b>Runoff routing and propagule transport</b>			
$\phi_{i,j}$	Fraction of overland flow from cell $i$ to downslope cell $j$	-	-
$A_i$	Upslope contributing area to $i$	L <sup>2</sup>	m <sup>2</sup>
$B$	Biomass density per area	M L <sup>-2</sup>	g m <sup>-2</sup>
$\delta$	Effective soil depth of interaction with overland flow	L	mm
$\chi_{ij}$	Euclidean distance between cells $i$ and $j$	L	m
$B_{runoff}$	Net change in biomass density as a result of overland flow	M L <sup>-2</sup>	g m <sup>-2</sup>
$h$	Depth of overland flow	L	m
$C$	Concentration of biomass in runoff	M L <sup>-3</sup>	g m <sup>-3</sup>
$q_c$	Water flux per unit width channel	L <sup>2</sup> T <sup>-1</sup>	m <sup>2</sup> day <sup>-1</sup>
$\alpha$	Tunable overland transport parameter	L <sup>-<math>\frac{1}{5}</math></sup> T <sup>-<math>\frac{2}{5}</math></sup>	m <sup>-<math>\frac{1}{5}</math></sup> day <sup>-<math>\frac{2}{5}</math></sup>
$\overline{u_{i,j}}$	Mean runoff velocity between $i$ and $j$	L T <sup>-1</sup>	m day <sup>-1</sup>
$C_{io}$	Concentration of biomass in runoff at source cell	M L <sup>-3</sup>	g m <sup>-3</sup>
$M_{ij}^+$	Deposited biomass at cell $j$ originating from $i$	M	g
$M_j^+$	Total deposited biomass at cell $j$	M	g
$u$	Runoff velocity	L T <sup>-1</sup>	m day <sup>-1</sup>
$K$	Kinematic resistance factor	L <sup><math>\frac{1}{3}</math></sup> T <sup>-1</sup>	m <sup><math>\frac{1}{3}</math></sup> day <sup>-1</sup>
$\nu$	Land surface flow resistance	L <sup>-<math>\frac{1}{3}</math></sup> T	m <sup>-<math>\frac{1}{3}</math></sup> day
$M_i^-$	Biomass mobilized from cell $i$	M	g
$\gamma_i$	Fraction of mobilized biomass from $i$ deposited in domain	-	-
$\ell$	Overland flow path coordinate	L	m
$\beta$	Sink strength rate parameter	T <sup>-1</sup>	day <sup>-1</sup>
$\bar{h}$	Spatially-averaged runoff depth	L	m
$v$	Aggregated velocity factor	L <sup><math>\frac{4}{5}</math></sup> T <sup>-<math>\frac{2}{5}</math></sup>	m <sup><math>\frac{4}{5}</math></sup> day <sup>-<math>\frac{2}{5}</math></sup>
$\overline{v_{i,j}}$	Spatially-averaged aggregated velocity factor	L <sup><math>\frac{4}{5}</math></sup> T <sup>-<math>\frac{2}{5}</math></sup>	m <sup><math>\frac{4}{5}</math></sup> day <sup>-<math>\frac{2}{5}</math></sup>
$\Delta \ell$	Flow path length within cell	L	m
$\overline{u_j}$	Storm-averaged runoff velocity at $j$	L T <sup>-1</sup>	m day <sup>-1</sup>
<b>Pathogen growth and diffusive spread</b>			
$r_{max}$	Maximum fractional growth rate at ambient temperature	-	-
$T_{soil}$	Soil temperature	K	°C
$m$	Pathogen growth soil moisture dependence factor	-	-
$r_o$	Pathogen fractional growth rate at T = 0°C	-	-
$\Delta r$	Pathogen growth rate temperature dependence	K <sup>-1</sup>	°C <sup>-1</sup>
$d$	Mortality rate	-	-
$B_{max}$	Steady state pathogen biomass density	M L <sup>-2</sup>	g m <sup>-2</sup>
$D_{max}$	Maximum pathogen diffusion coefficient	L <sup>2</sup> T <sup>-1</sup>	m <sup>2</sup> day <sup>-1</sup>

Table 2: Variables and parameters used across all components of the model

## 3 Model parameterization and tests

### 3.1 Site descriptions

Two Pc infections, one in a *Banksia* woodland growing on the deep sands of the Swan Coastal Plain in Western Australia, and one in an *Erica* heathland located in the Sierra de las Villuercas mountain range in eastern Extremadura, Spain, form case studies where we test whether the model can represent the spatial spread of Pc and the potential role overland flow plays in this spread.

#### 3.1.1 Western Australian site

The Western Australian case study site is a Pc infection established before 1950 in *Banksia* woodlands growing on the flat, deep sands of the Swan Coastal Plain, north of the city of Perth in Western Australia. Wilson et al. (2012) mapped (and ground-truthed) the spatial progression of Pc infection at the site from 1953 - 2008 from aerial imagery, providing the spatial dataset we analyzed. The site has a warm Mediterranean climate with 725 mm/year precipitation, average summer high temperatures of 32 °C and average winter low temperatures of 9 °C. Climate data (precipitation and temperature) were obtained from the nearby Pearce RAAF Base weather station (Station ID 009053, <http://www.bom.gov.au/climate/data/>). Daily maximum and minimum temperatures were used to compute potential evaporation via Hargreaves' equation (Hargreaves et al., 1985). Climate gap filling used average temperature data (for the given day of year in all other years), and a satellite weather product (CHIRPS, version 2.0 final) for daily rainfall (Funk et al., 2015). A 5×5 m, LiDAR-derived DEM for the site (Geoscience Australia, 2015) was interpolated onto a 1 m grid.

#### 3.1.2 Spanish site

The Spanish case study site is a Pc infection established before 1981 in the *Erica* heathlands of the the Montes de Toledo on the Spanish central plateau. The fairly shallow, poorly drained quartzitic ultisols, and deeply incised landscape (slope gradients of 5% - 50%) contrasts sharply with the Western Australian site. Cardillo et al. (2018) mapped disease foci and their expansion from aerial photography at this site to determine spatial progression of disease from 1981 -2012, providing the spatial dataset we used for this site. This site also has a warm Mediterranean climate, with an average of 855 mm/year precipitation, average summer high temperatures of temperatures of 32 °C and average winter low temperatures of 4 °C based on climate data obtained from the nearby Cañamero weather station (Station ID 4334, Agencia Estatal de Meteorología AEMET). The same ET estimation and climate record gap filling procedures were employed as in Western Australia. A 5×5 m DEM (PNOA-MDT05 2010 CC-BY 4.0 [ign.es](http://ign.es)) for the site was obtained from the Instituto Geográfico Nacional (IGN, Spain) and interpolated onto a 1 m grid.

### 3.2 Selection of disease patches to model

We identified isolated disease patches that did not initially intersect roads, bare patches or other barriers to Pc dispersal. Where patch growth caused the patch to intersect channels or other unvegetated areas, we treated those features as boundaries, forcing Pc biomass to remain zero on the other side of the boundaries. The locations of these features was identified using the D- $\infty$  algorithm to map upslope contributing area, and corroborated against aerial imagery. With these constraints, eight patches (patches a-h) were selected from Warbrook Road in Western Australia. Patch sizes were measured in 1987 and 1992, defining a 5-year time domain for running the model. Seven patches (patches 1-7) were selected from the Spanish observations, three (patches 1-3) measured between 1981 and 1984, and four (patches 4-7) between 2010 and 2012.

### 3.3 Numerical implementation

Within each observed disease patch the model was initialized with  $B = B_{max}$ . Soil moisture was initialized using a one year spin-up starting at the end of the dry season, when it was assumed  $s = s_{wp}$ . The model was implemented on a two-dimensional spatial grid (1m x 1m) that aligned with the DEM grid, using a 1 day time step (we confirmed that results were stable to changes in the time and space grids). A centered difference scheme was used for the second-order spatial terms from the diffusion equation. An explicit (forward) scheme was used for time stepping. Open flux boundary conditions were assumed, with one-sided difference schemes used at the spatial boundaries. The D- $\infty$  algorithm was implemented using tools developed by Eddins (2018). Model output, consisting of the Pc biomass density ( $B(x, y, t)$ ) was binarized at a threshold of  $B = 0.5B_{max}$ , to allow comparison to mapped infection boundaries (Figure 2D).

### 3.4 Parameterization

In Western Australia, we modeled the 1.5 m deep root zone containing most *Banksia* roots (Hill et al., 1994), with a freely-draining bottom boundary (accounting for the, on average, 8 m of unsaturated sand overlying the water table at this site). For the Spanish sites, we modeled the 0.7 m deep soil with an impermeable bottom boundary representing a low permeability B horizon (Espejo, 1987). Hydraulic parameters for the soils were taken from Laio et al. (2001) using the “sand” for Western Australia and “sandy loam” for Spain. These soils types were used to determine the effective depth of interaction ( $\delta$ ) following Ahuja et al. (1981).

The fractional pathogen growth rate at 0 °C ( $r_0$ ) was set to  $-0.171 \text{ day}^{-1}$  (Malajczuk et al., 1979). Given the relatively shallow soil depths, we approximated  $T_{soil}$  with  $T_{air}$  at all times for both sites. The moisture dependence of the growth ( $m(s)$ ) was estimated as a piecewise function based on experimental

data from Malajczuk et al. (1979) (Appendix B.1).

### 3.5 Calibration

Four model parameters needed to be calibrated to run the model: the mortality rate ( $d$ ), diffusion coefficient ( $D_{max}$ ), temperature dependence of growth ( $\Delta r$ ), and the overland transport parameter ( $\alpha$ ). We estimated plausible ranges for the pathogen mortality rate ( $d$ ) from Hwang et al. (1978), of growth temperature dependence  $\Delta r$  from Thompson et al. (2014) and Malajczuk et al. (1979), of maximum diffusion coefficient  $D_{max}$  from patch growth rates in the upslope direction (assumed to be due to purely diffusive transport). The combined pathogen sink rate constant and land surface roughness parameter  $\alpha$  is poorly constrained a priori, so several orders of magnitude of  $\alpha$  values were screened to find a plausible range for calibration.

#### 3.5.1 Calibration metrics

Model calibration aimed to maximize agreement between mapped observations of the spatial extent of Pc infection and predictions for each patch, focusing on four features: the orientation of the disease patch, its eccentricity, the length of its major axis, and an areal growth increment. Differences between these features and observations were computed, and standardized to lie between 0 (complete disagreement) and 1 (perfect agreement). Fitting, differencing and standardization of the features are described in the Appendix C. The four standardized scores were averaged to give a composite score for each modeled patch.

#### 3.5.2 Calibration and Model Experiments

We calibrated the growth and diffusion related parameters  $\Delta r$ ,  $D_{max}$ , and  $d$  together for each site (i.e. these parameters were common to every patch at the site).

We did this for two cases: one in which overland flow transport of Pc was omitted (the “diffusion optimized” case), and one in which overland flow transport of Pc was included. In the diffusion optimized case, we ran the calibration in two stages - firstly sampling parameter values from a coarse factorial grid spanning the range of plausible values, and secondly sampling over a finer range of values identified after the first step. No constraints were placed upon the parameter values, and the refinement process was continued until an optimum value of each parameter was found, such that changing the value of any parameter while holding the others constant resulted in a decrease in the mean composite score. Combinations of site-wide parameters were tested and the scores averaged for a range of  $\alpha$  values. Once the values of these site-wide parameters were determined, we then further calibrated  $\alpha$  individually for each patch to account for differences in surface cover across the landscape.

We used the two versions of the calibrated model to firstly identify whether, and at which sites, including overland transport resulted in an improved description of patch growth geometry relative to a model with only diffusive spread included. For those sites where overland transport did improve the model performance, we re-ran the calibrated (overland flow) models, but ‘turned off’ overland transport. The differences in predictions provide a measure of the importance of within-soil versus overland flow driven spread of Pc.

## 4 Results

The results of the experiments are summarized in Figure 4, which shows model predictions for select patches from Western Australia (panels A and B) and Spain (panels C and D) and the compiled patch scores from the different experiments (panels E and F). Results for all other patches are shown in Appendices E and F and the fitted parameters are reported in G. The distribution of modeled soil moisture values at both sites is shown in Appendix H.

No overland flow occurred in Western Australia, so there was no differentiation between the versions of the model with and without overland transport of Pc. The model made very good predictions of Pc spread, with a mean composite score of 0.856 across the 8 patches (Figure 4E). It was not able to capture the exact borders of the disease patches, which are generally uneven and asymmetric in the observed data.

Intermittent episodes of overland flow were predicted for the Spanish site. Including a representation of Pc transport in this overland flow improved model performance (mean improvement of 0.149 in the composite score), relative to the diffusion optimized case (Figure 4F). With overland flow included, the model performance was comparable to that in Western Australia, with an average composite score of 0.864 (Figure 4E). For two patches (blue dots - Figures 4E and 4F) little to no improvement resulted from adding overland transport. These patches also had the lowest composite scores in the overland transport model (Figure 4E). The patches where overland transport improved predictions (red dots - Figures 4E and 4F) the mean composite score of was higher (0.876 for the overland transport model) and resulted from more improvement (0.204) over the diffusion optimized calibration.

Turning overland flow off in the calibrated model for the Spanish patches lead to a notable degradation in model performance (Figure 4F), with the exception of the two patches (blue dots) which were insensitive to overland flow during calibration. In the other patches, excluding overland transport lowered the composite score by an average of 0.220.

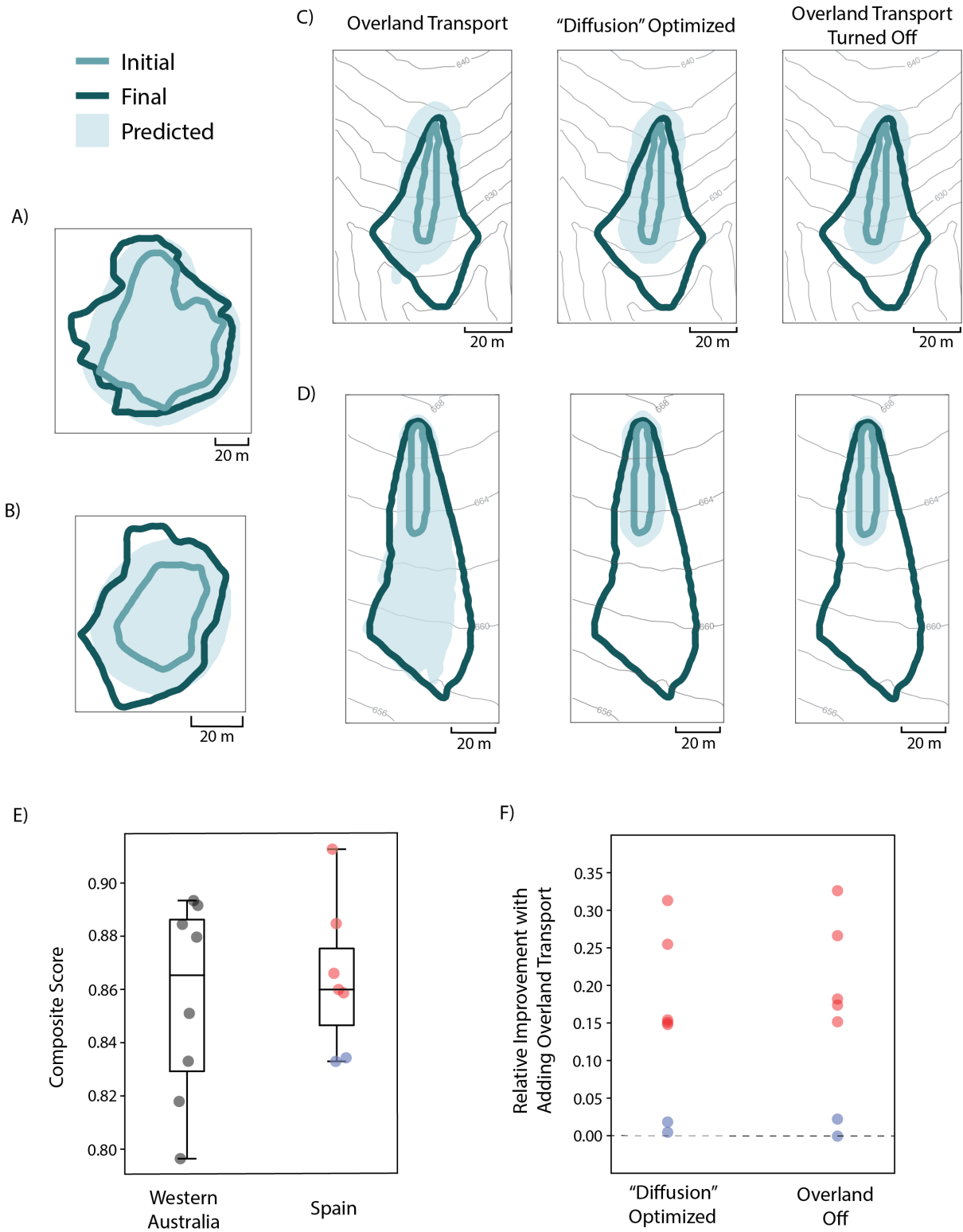


Figure 4: Model output from the Western Australia site for Patch b (A) and Patch a (B), with observed initial and final patch extents outlined and model predictions shaded. Model predictions for the different model configurations tested at the Spanish site are shown for Patch 2 (C) and Patch 7 (D). Composite scores of all patches for the model configuration allowing for overland transport are shown for both sites in (E), with the Spanish patches subset into patches that varied greatly between configurations (red dots) and those that had minimal variation (blue dots). For the Spanish site, the improvements in composite scores for each patch with adding overland transport relative to the other configurations are shown in (F), with the color scheme continued from (E).

## 5 Discussion and Conclusions

Although climatically similar, the different soil conditions at the Western Australian and Spanish sites resulted in very different hydrological dynamics: soils never approached saturation and no runoff occurred on the deep Western Australian sands, while soils in the Spanish site approached saturation and generated runoff during the winter rainy season.

These differing hydrological processes lead to different requirements in simulating Pc spread. There was a strong agreement between model predictions and observations of disease spread in Western Australia, suggesting that the biomass growth and diffusion components of the model work effectively to describe Pc spread from disease foci.

In the Spanish sites, overland flow transport needed to be included to represent the growth of most of the patches, excluding two which appeared to be insensitive to overland flow. If the diffusive model were calibrated on sites with no overland flow and then applied to model Pc in a location similar to the Spanish site, Pc spread rates would be underestimated - in this case by a matter of 350 m<sup>2</sup>/year on average.

Model limitations included the difficulty of simulating patch edges in Western Australia, which may be due to omitted heterogeneities in soil and host properties, as well as to the difficulty of detecting disease at patch boundaries. Further, limitations of the data used to parameterize the model domain may be related to the apparent lack of importance of overland flow in two of the modeled Spanish sites. For example, Patch 2 (Figure 4C) is located on a ridgeline in the landscape, and its growth occurs across the ridge: local, flat topography in this area may not have been well resolved in the original 5 m × 5 m DEM used to represent the site. Indeed, simulations tended to be biased towards spread on one side of the ridge - as would be expected if the DEM failed to resolve a correct ridge location within the patch. The use of a coarse DEM may also be responsible for several simulations where the model fails to represent the correct shape of the Pc patch (e.g. Patches 1 and 4).

Additionally, the model omitted other transport pathways, notably spread via vectors (relevant considering the Spanish site is used as goat pasture), and transport within the soil. Considering that the model generally underestimated Pc spread in the patches where its performance was poor, additional transport mechanisms could be responsible.

Overall, the modeling results demonstrate the feasibility of describing the spatiotemporal dynamics of Pc spread provided information about the rhizosphere and transport mechanisms is available. Further, it showed how hydrological processes can act as a driver of disturbance caused by plant pathogens, with the overland runoff generation at the Spanish site introducing a relatively rapid and long-distance transport mechanism for Pc. Models of pathogen growth and spread such as the one presented here could be readily incorporated into scenario planning around water and drainage management - for example by coupling this model to distributed hydrological models already in use. Alternatively, some of the key



dynamics revealed in this study can be used to suggest ways to augment Pc risk assessments to account for potential transport via overland flow in addition to the simple annual climate, soil and slope metrics that are currently used to describe disease risk. For example, Porporato et al. (2004) showed that the probability of soils saturating is controlled by two dimensionless ratios: the soil water holding capacity to the average storm depth, and the ratio of the mean rate of water input (e.g. average storm depth multiplied by average time between storms) to the rate of water loss by evaporation. These ratios can be readily calculated (on a seasonal basis) to identify the likelihood of saturation, and therefore overland flow events. Where saturation is more topographically than edaphically controlled, metrics such as the topographic wetness index (TWI) (Beven et al., 1979), could be incorporated into risk assessments. Flow routing algorithms (like the one used in this model) could be used to assess how far disease propagules mobilized at a given site in a landscape could be transported if overland flow does occur. Together, these kinds of measures suggest the possibility of identifying sites at high risk of supporting new disease and sites at high risk of spreading disease to new locations - and thus potentially new ways to triage and manage Pc risk - at least as far as that risk is driven by local hydrological factors.

Pc already presents a major risk to plant communities around the globe, and this threat is likely to increase as Pc extends into new regions with climate change (Thompson et al., 2014). Here, for the first time, we modeled the spatio-temporal dynamics of Pc infected patches where spread was driven by local biological and hydrological processes. The results demonstrated a notable role for surface hydrology in accelerating and directing Pc infection spread over timescales of years, indicating how hydrology can act as a driver of disturbance from plant pathogens. Adjusting existing risk management frameworks to account for the influence of local hydrology on spread behavior could provide a new target for Pc control. Further, while this modeling study focused on Pc, Pc is one of many plant pathogens that spreads in moist soil. Thus, there is the potential to apply this framework to better understand and manage disturbances caused by other pathogens.

## 6 Acknowledgements

We thank Janine Kinloch, Barbara Wilson, Katherine Zdunic, and the Western Australia Department of Biodiversity, Conservation and Attractions (DBCA) for providing the disease mapping data for the site in Western Australia. This work was supported by a National Science Foundation Graduate Research Fellowship [Grant No. DGE 1752814 to JVV]; the Junta de Extremadura [Grant No. GR18079 to EA]; the Spanish Agencia Estatal de Investigación [Grant No. FIS2016-76359-P (partially financed with FEDER funds) to EA]; and the National Institute of Agricultural Research of Spain [Grant No. INIA RTA 2014-00063-C01 to EC]. Compiled patch data and climate data used in the model and collected from sources as discussed in the text are available at <http://www.hydroshare.org/>

resource/a010a9c248284240a44180d339a2cba2/. All model code is available at [https://github.com/jvwilkening/Pc\\_Spread\\_Model](https://github.com/jvwilkening/Pc_Spread_Model).

## References

- Ahuja, L R et al. (1981). “The Depth of Rainfall-Runoff-Soil Interaction as Determined by 32P”. In: *Water Resources Research* 17.4, pp. 969–974.
- Andow, DA et al. (1990). “Spread of invading organisms”. In: *Landscape Ecology* 4.2-3, pp. 177–188.
- Batini, FE et al. (1980). “An examination of the effects of changes in catchment condition on water yield in the Wungong catchment, Western Australia.” In: *Australian Forest Research* 10.1, pp. 29–38.
- Benjamin, M and FJ Newhook (1982). “Effect of glass microbeads on Phytophthora zoospore motility”. In: *Transactions of the British Mycological Society* 78.1, pp. 43–46.
- Bergot, Magali et al. (2004). “Simulation of potential range expansion of oak disease caused by Phytophthora cinnamomi under climate change”. In: *Global Change Biology* 10.9, pp. 1539–1552.
- Beven, Keith J and Michael J Kirkby (1979). “A physically based, variable contributing area model of basin hydrology”. In: *Hydrological Sciences Journal* 24.1, pp. 43–69.
- Boyer, John S (1995). “Biochemical and biophysical aspects of water deficits and the predisposition to disease”. In: *Annual Review of Phytopathology* 33.1, pp. 251–274.
- Brasier, Clive M (1996). “Phytophthora cinnamomi and oak decline in southern Europe. Environmental constraints including climate change”. In: *Annales des Sciences Forestieres*. Vol. 53. 2-3. EDP Sciences, pp. 347–358.
- Brooks, R and T Corey (1964). “Hydraulic properties of porous media”. In: *Hydrology Papers, Colorado State University* 24, p. 37.
- Brutsaert, Wilfried et al. (2005). *Hydrology: an introduction*. Cambridge University Press.
- Burgess, Treena I et al. (2017). “Current and projected global distribution of Phytophthora cinnamomi, one of the world’s worst plant pathogens”. In: *Global Change Biology* 23.4, pp. 1661–1674.
- Cardillo, Enrique, Angel Acedo, and Enrique Abad (2018). “Topographic effects on dispersal patterns of Phytophthora cinnamomi at a stand scale in a Spanish heathland”. In: *PloS one* 13.3, e0195060.
- Chakraborty, Sukumar, AV Tiedemann, and Paul S Teng (2000). “Climate change: potential impact on plant diseases”. In: *Environmental pollution* 108.3, pp. 317–326.
- Clapp, Roger B and George M Hornberger (1978). “Empirical equations for some soil hydraulic properties”. In: *Water resources research* 14.4, pp. 601–604.
- Colhoun, John (1973). “Effects of environmental factors on plant disease”. In: *Annual Review of Phytopathology* 11.1, pp. 343–364.

- Commonwealth of Australia (2014). *Background: threat abatement plan for disease in natural ecosystems caused *Phytophthora cinnamomi**. Tech. rep.
- Cook, RJ and RI Papendick (1972). “Influence of water potential of soils and plants on root disease”. In: *Annual Review of Phytopathology* 10.1, pp. 349–374.
- Crist, CR, DF Schoeneweiss, et al. (1975). “The influence of controlled stresses on susceptibility of European white birch stems to attack by *Botryosphaeria dothidea*.” In: *Phytopathology* 65.4, pp. 369–373.
- Cunniffe, Nik J. and Christopher A. Gilligan (2008). “Scaling from mycelial growth to infection dynamics: a reaction diffusion approach”. In: *Fungal Ecology* 1.4, pp. 133–142. ISSN: 17545048. DOI: 10.1016/j.funeco.2008.10.007. URL: <http://dx.doi.org/10.1016/j.funeco.2008.10.007>.
- Dawson, Peter and Gretna Weste (1985). “Changes in the distribution of *Phytophthora cinnamomi* in the Brisbane Ranges National Park between 1970 and 1980-81”. In: *Australian Journal of Botany* 33.3, pp. 309–315.
- Desprez-Loustau, Marie-Laure et al. (2006). “Interactive effects of drought and pathogens in forest trees”. In: *Annals of forest science* 63.6, pp. 597–612.
- Dickenson, Susan and BEJ Wheeler (1981). “Effects of temperature, and water stress in sycamore, on growth of *Cryptostroma corticale*”. In: *Transactions of the British Mycological Society* 76.2, pp. 181–185.
- Dunne, Thomas and Richard D Black (1970). “Partial area contributions to storm runoff in a small New England watershed”. In: *Water resources research* 6.5, pp. 1296–1311.
- Eddins, S (2018). *Upslope Area Functions*. <https://www.mathworks.com/matlabcentral/fileexchange/15818-upslope-area-functions>. (Visited on ).
- Espejo, R (1987). “The soils and ages of the “raña” surfaces related to the Villuercas and Altamira mountain ranges (Western Spain)”. In: *Catena* 14.5, pp. 399–418.
- Ferrin, DM and ME Stanghellini (2006). “Effect of water potential on mycelial growth and perithecial production of *Monosporascus cannonballus* in vitro”. In: *Plant pathology* 55.3, pp. 421–426.
- Flower, Charles E and Miquel A Gonzalez-Meler (2015). “Responses of temperate forest productivity to insect and pathogen disturbances”. In: *Annual review of plant biology* 66, pp. 547–569.
- Funk, Chris et al. (2015). “The climate hazards infrared precipitation with stations—a new environmental record for monitoring extremes”. In: *Scientific data* 2, p. 150066.
- Geoscience Australia (2015). *Digital Elevation Model (DEM) of Australia derived from LiDAR 5 Metre Grid*. <http://pid.geoscience.gov.au/dataset/ga/89644>.
- Gómez-Paccard, Clara et al. (2015). “Soil–water relationships in the upper soil layer in a Mediterranean Paleixerult as affected by no-tillage under excess water conditions—influence on crop yield”. In: *Soil and Tillage Research* 146, pp. 303–312.

- Hardham, Adrienne R and Leila M Blackman (2018). “Phytophthora cinnamomi”. In: *Molecular plant pathology* 19.2, pp. 260–285.
- Hargreaves, George H and Zohrab A Samani (1985). “Reference crop evapotranspiration from temperature”. In: *Applied engineering in agriculture* 1.2, pp. 96–99.
- Hill, TCJ, JT Tippett, and BL Shearer (1994). “Invasion of Bassendean dune Banksia woodland by Phytophthora cinnamomi”. In: *Australian Journal of Botany* 42.6, pp. 725–738.
- Horton, Robert E (1933). “The role of infiltration in the hydrologic cycle”. In: *Eos, Transactions American Geophysical Union* 14.1, pp. 446–460.
- Hwang, S C and W H Ko (1978). “Biology of chlamydospores, sporangia, and zoospores of Phytophthora cinnamomi in soil”. In: pp. 726–731.
- Jung, T, IJ Colquhoun, and GE St J Hardy (2013). “New insights into the survival strategy of the invasive soilborne pathogen P hytophthora cinnamomi in different natural ecosystems in W estern A ustralia”. In: *Forest Pathology* 43.4, pp. 266–288.
- Jung, T and G Dobler (2002). “First report of littleleaf disease caused by Phytophthora cinnamomi on Pinus occidentalis in the Dominican Republic”. In: *Plant disease* 86.11, pp. 1275–1275.
- Kinal, J, BL Shearer, RG Fairman, et al. (1993). “Dispersal of Phytophthora cinnamomi through lateritic soil by laterally flowing subsurface water.” In: *Plant Disease* 77.11, pp. 1085–1090.
- Kliejunas, J. T. and W H Ko (1976). “Dispersal of Phytophthora cinnamomi on the Island of Hawaii”. In: *Ecology and Epidemiology* 66, pp. 457–460.
- Laio, F et al. (2001). “Plants in water-controlled ecosystems : active role in hydrologic processes and response to water stress II . Probabilistic soil moisture dynamics”. In: 24.
- Lowe, Sarah et al. (2000). *100 of the world’s worst invasive alien species: a selection from the global invasive species database*. Vol. 12. Invasive Species Specialist Group Auckland.
- Madar, Z, Z Solel, M Kimchi, et al. (1989). “Effect of water stress in cypress on the development of cankers caused by Diplodia pinea f. sp. cupressi and Seiridium cardinale.” In: *Plant Disease* 73.6, pp. 484–486.
- Malajczuk, N and C Theodorou (1979). “Influence of water potential on growth and cultural characteristics of Phytophthora cinnamomi”. In: *Transactions of the British Mycological Society* 72.1, pp. 15–18.
- Marçais, B, F Dupuis, and ML Desprez-Loustau (1996). “Modelling the influence of winter frosts on the development of the stem canker of red oak, caused by Phytophthora cinnamomi”. In: *Annales des sciences forestières*. Vol. 53. 2-3. EDP Sciences, pp. 369–382.
- National Heritage Trust and Environment Australia (2001). *Threat abatement plan for dieback caused by the root-rot fungus Phytophthora cinnamomi*. Tech. rep.

- Okubo, Akira and Smon A Levin (2013). *Diffusion and ecological problems: modern perspectives*. Vol. 14. Springer Science & Business Media.
- Oudemans, Peter V (1999). “Phytophthora species associated with cranberry root rot and surface irrigation water in New Jersey”. In: *Plant Disease* 83.3, pp. 251–258.
- Park, Andrew W, Simon Gubbins, and Christopher A Gilligan (2001). “Invasion and persistence of plant parasites in a spatially structured host population”. In: *Oikos* 94.1, pp. 162–174.
- Podger, FD (1972). “Phytophthora cinnamomi, a Cause of Lethal Disease in Indigenous Plant Communities in Western Australia”. In: *Phytopathology* 62, pp. 972–981.
- Porporato, Amilcare, Edoardo Daly, and Ignacio Rodriguez-Iturbe (2004). “Soil water balance and ecosystem response to climate change”. In: *The American Naturalist* 164.5, pp. 625–632.
- Reeser, Paul W et al. (2011). “Phytophthora species in forest streams in Oregon and Alaska”. In: *Mycologia* 103.1, pp. 22–35.
- Ristaino, Jean Beagle and Marcia L Gumpertz (2000). “New frontiers in the study of dispersal and spatial analysis of epidemics caused by species in the genus Phytophthora”. In: *Annual Review of Phytopathology* 38.1, pp. 541–576.
- Salama, Ramsis B, Richard Silberstein, and Daniel Pollock (2005). “Soils characteristics of the Bassendean and Spearwood Sands of the Gnangara Mound (Western Australia) and their controls on recharge, water level patterns and solutes of the Superficial Aquifer”. In: *Water, Air, & Soil Pollution: Focus* 5.1-2, pp. 3–26.
- Schober, BM and JC Zadoks (1999). “Water and temperature relations of softrot bacteria: growth and disease development”. In: *Annals of applied biology* 134.1, pp. 59–64.
- Schofield, NJ, GL Stoneman, and IC Loh (1989). “Hydrology of the jarrah forest”. In: *The jarrah forest*. Springer, pp. 179–201.
- Shea, SR et al. (1983). “Distribution, reproduction, and movement of Phytophthora cinnamomi on sites highly conducive to jarrah dieback in south Western Australia.” In: *Plant Disease* 67.9, pp. 970–973.
- Shearer, BL, CE Crane, and A Cochrane (2004). “Quantification of the susceptibility of the native flora of the South-West Botanical Province, Western Australia, to Phytophthora cinnamomi”. In: *Australian Journal of Botany* 52.4, pp. 435–443.
- Shearer, BL, SR Shea, and PM Deegan (1987). “Temperature-growth relationships of Phytophthora cinnamomi in the secondary phloem of roots of Banksia grandis and Eucalyptus marginata.” In: *Phytopathology* 77.5, pp. 661–665.
- Suleman, Patrice, Azza Al-Musallam, and Cynthia A Menezes (2001). “The effect of solute potential and water stress on black scorch caused by Chalara paradoxa and Chalara radicola on date palms”. In: *Plant disease* 85.1, pp. 80–83.

- Tarboton, DG (1997). “A new method for the determination of flow directions and upslope areas in grid digital elevation models”. In: *Water Resources Research* 33.2, pp. 309–319.
- Thompson, Sally E, Simon Levin, and Ignacio Rodriguez-Iturbe (2013). “Linking plant disease risk and precipitation drivers: a dynamical systems framework”. In: *The American Naturalist* 181.1, E1–E16.
- (2014). “Rainfall and temperatures changes have confounding impacts on *Phytophthora cinnamomi* occurrence risk in the southwestern USA under climate change scenarios”. In: *Global change biology* 20.4, pp. 1299–1312.
- Thomson, SV, RM Allen, et al. (1974). “Occurrence of *Phytophthora* species and other potential plant pathogens in recycled irrigation water.” In: *Plant Disease Reporter* 58.10, pp. 945–949.
- Vettraino, AM et al. (2005). “Occurrence and distribution of *Phytophthora* species in European chestnut stands, and their association with Ink Disease and crown decline”. In: *European Journal of Plant Pathology* 111.2, p. 169.
- Weste, Gretna M and P Taylor (1971). “The invasion of native forest by *Phytophthora cinnamomi*. I. Brisbane Ranges, Victoria”. In: *Australian Journal of Botany* 19.3, pp. 281–294.
- Weste, Gretna and Ceridwen Law (1973). “The invasion of native forest by *Phytophthora cinnamomi*. III. Threat to the National Park, Wilson’s Promontory, Victoria”. In: *Australian Journal of Botany* 21.1, pp. 31–51.
- Weste, Gretna, Pamela Ruppin, and Kumudini Vithanage (1976). “*Phytophthora cinnamomi* in the Brisbane Ranges: patterns of disease extension”. In: *Australian Journal of Botany* 24.2, pp. 201–208.
- Wilson, Barbara A et al. (2012). “Use of remote sensing to map occurrence and spread of *Phytophthora cinnamomi* in *Banksia* woodlands on the Gnangara Groundwater System, Western Australia”. In: *Australian Journal of Botany* 60.6, pp. 495–505.
- Xu, C, RP Silberstein, and AD Barr (2003). “Estimates of groundwater recharge beneath *Banksia* woodland on the Swan Coastal Plain using a vertical flux model (WAVES): sensitivity analysis”. In: *MODSIM 2003 Proceedings of International Congress on Modelling and Simulation. International Modelling and Simulation Society, Townsville, Queensland*, pp. 177–182.

# Appendices

## A Conservation of Pathogen Mass with Flow Outside Model Domain

To account for possible transport outside the domain, the fraction of biomass accounted for within the domain that originated at  $i$ ,  $\gamma_i$ , is found:

$$\gamma_i = \frac{\sum_{j=1}^n \frac{e^{-\frac{\alpha \chi_{i,j}}{\bar{v}_{i,j}}}}{v_j} \phi_{i,j}}{\sum_{j=1}^{\infty} \frac{e^{-\frac{\alpha \chi_{i,j}}{\bar{v}_{i,j}}}}{v_j} \phi_{i,j}} \quad (\text{A.1})$$

where  $n$  is the number of down-gradient cells within the modeled domain. For the theoretical limit of  $\infty$  down-gradient cells, the sum is computed using  $\Delta x$  as the increment in distance between the cells ( $\chi_{i,j}$ ) and the velocities,  $v_j$  and  $\bar{v}_{i,j}$ , are approximated using the respective averages of those values within the modeled domain. This sum is computed until the incremental change in the sum with each additional term falls below a prescribed threshold value (set to 0.00001 in this case). This value can then be used in the calculation of  $C_{io}$  as derived in the main text:

$$C_{io} = \frac{B_i \delta \Delta x \Delta y}{z_r} \left( \sum_{j=1}^n \frac{\alpha e^{-\frac{\alpha \chi_{i,j}}{\bar{v}_{i,j}}} \Delta x q_{storm} A_i \phi_{i,j} t_{storm}}{v_j} \right)^{-1} \quad (\text{A.2})$$

## B Moisture Dependence of Growth

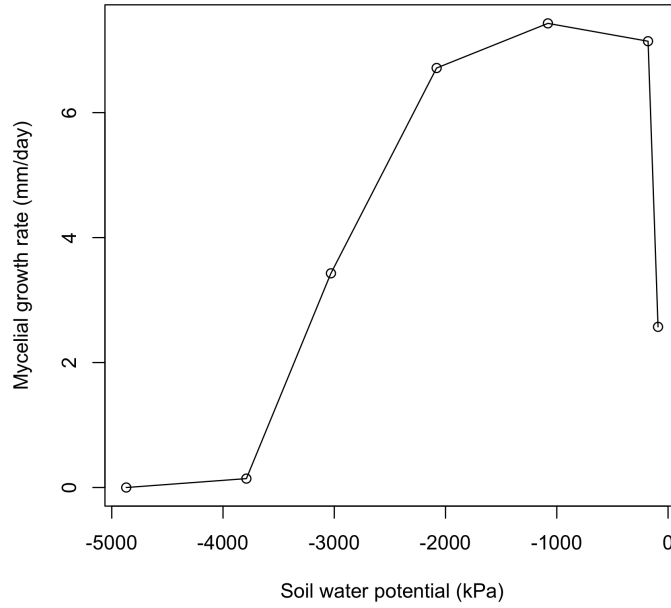


Figure B.1: A piecewise function of the moisture-dependence of pathogen growth [ $m(s)$ ] was found by linearly fitting segments to the data of Malajczuk et al., 1979

## C Patch Image Analysis

Using the image analysis tools in Matlab, an ellipse is fit to the infected cells ( $B \geq 0.5B_{max}$ ) such that the ellipse has the same normalized second moment of mass as the disease patch. With this fitted ellipse, the major axis, orientation, and eccentricity are then calculated.

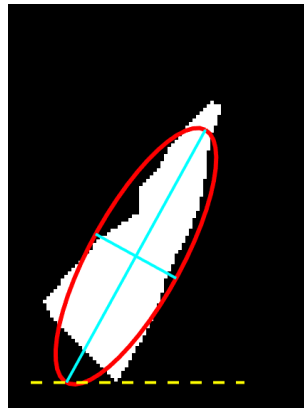


Figure C.1: For each patch of diseased cells (shown in white), an ellipse (red) is fitted. The major and minor axes of the ellipse (blue) are then found and further used to calculate the eccentricity. The orientation is determined as the angle between the major axis and the horizontal plane (dotted yellow).



## D Calculation of Composite Score

A composite score that quantifies how each patch prediction compares to the observed patch is calculated as the average of the following four components. The first three component scores use metrics from the ellipse fitting as described in C. For each of the individual components, as well as the overall score, the values range from 0 (poor match to observations) to 1 (perfect match to observations).

### Orientation score:

The orientation (degrees) of the major axis of the fitted ellipses is measured in degrees in the x-y plane. The differences between orientation for model and observations is computed, normalized by the half circle and differenced from one (to ensure that a score that is closer to one represents better model-observation agreement):

$$OS = 1 - \frac{|\text{Modeled Orientation} - \text{Observed Orientation}|}{180} \quad (\text{D.1})$$

### Major axis score:

The length of the major axes of the patches are compared and standardized by the observed major axis length, as:

$$MS = 1 - \frac{|\text{Modeled Major Axis Length} - \text{Observed Major Axis Length}|}{\text{Observed Major Axis Length}} \quad (\text{D.2})$$

### Eccentricity score:

The eccentricity (-) of the fitted ellipse is calculated as the distance from the center of the ellipse to the focus divided by one-half the major axis length. It will be equal to 0 for a perfect circle and 1 for a line and in terms of the major and minor axis lengths this is:

$$Eccentricity = \frac{\sqrt{(0.5 \times \text{major axis})^2 + (0.5 \times \text{minor axis})^2}}{0.5 \times \text{major axis}} \quad (\text{D.3})$$

The eccentricities are compared between model and observations, to form a standardized score:

$$ES = 1 - |\text{Modeled Eccentricity} - \text{Observed Eccentricity}| \quad (\text{D.4})$$

**Growth area:** The growth score assesses how well the model predicts where new pathogen growth will occur, relative to how much it overpredicts disease spread. The actual observed growth is tabulated as the number of model grid cells where new pathogen growth is observed between the initial and final observation points. The correctly predicted cells are the number of these cells which the model correctly predicts as being infected by Pc. The number of false positives is tabulated as the number of cells for which the model predicted pathogen growth but there was no observed pathogen present in the aerial photos. These are combined to calculate the growth score as:

$$GS = \frac{\# \text{ cells new growth correctly predicted}}{\# \text{ cells actual new growth observed} + \# \text{ cells with false positives}} \quad (\text{D.5})$$

## E All Western Australia Patch Predictions

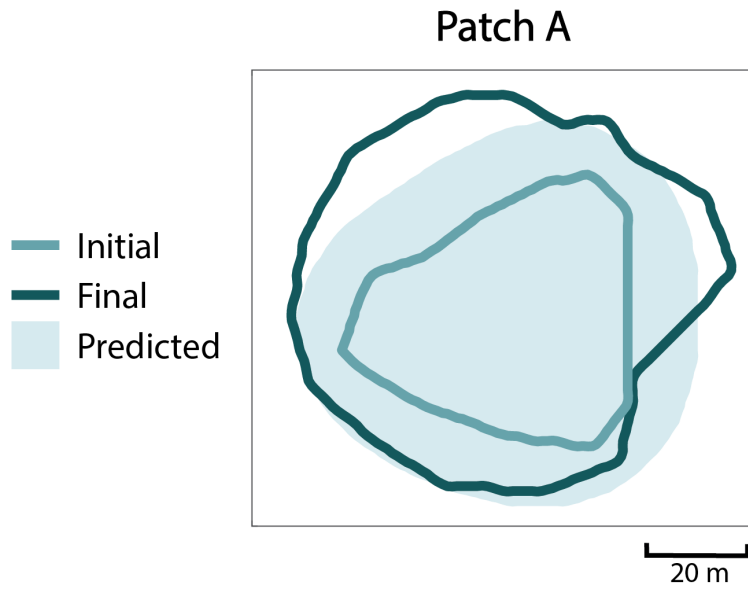


Figure E.1: Composite score of 0.892

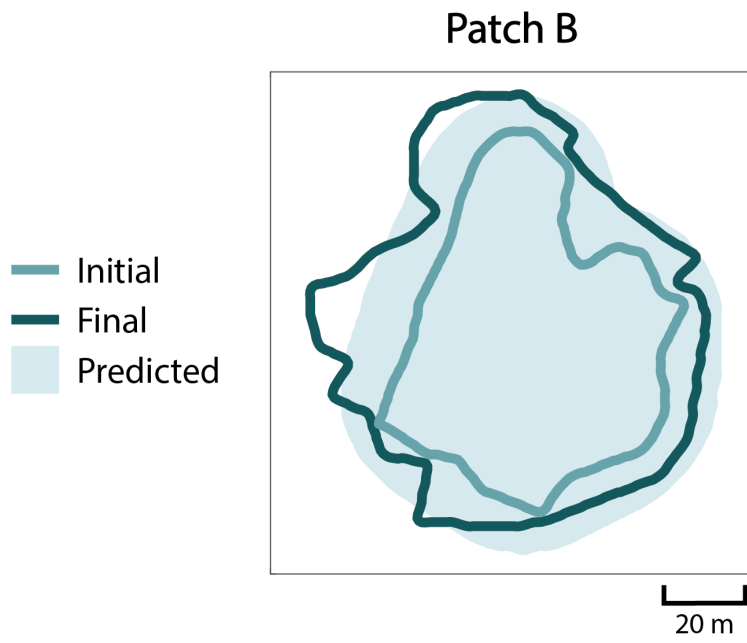


Figure E.2: Composite score of 0.884

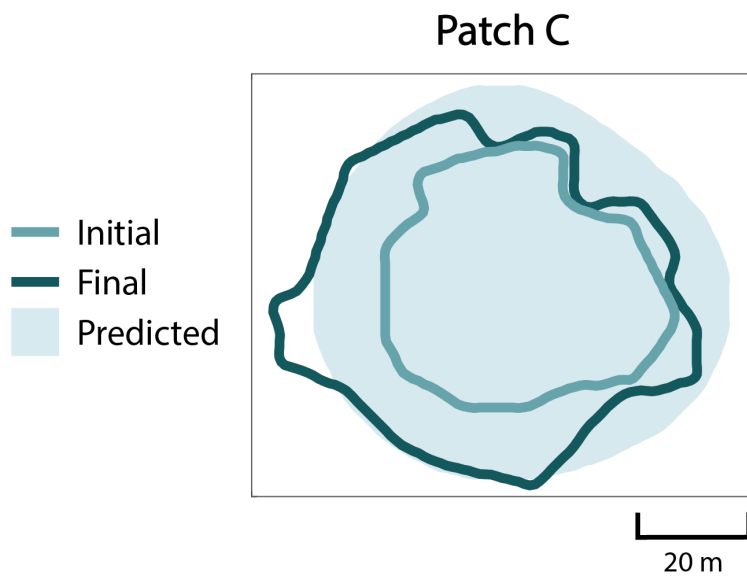


Figure E.3: Composite score of 0.851

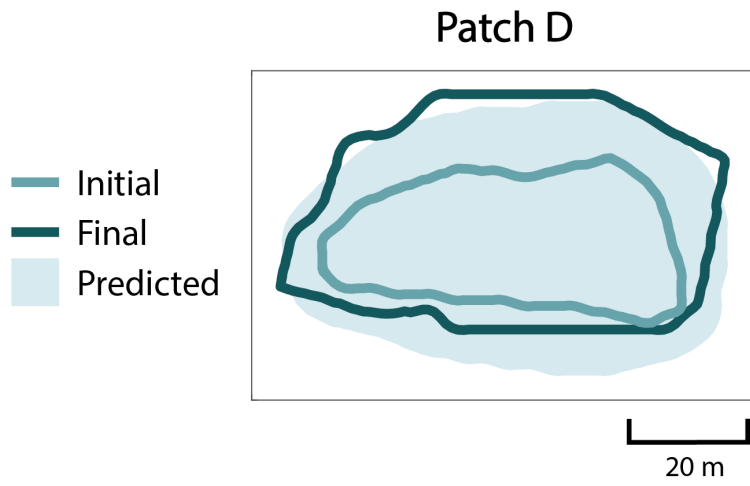


Figure E.4: Composite score of 0.893

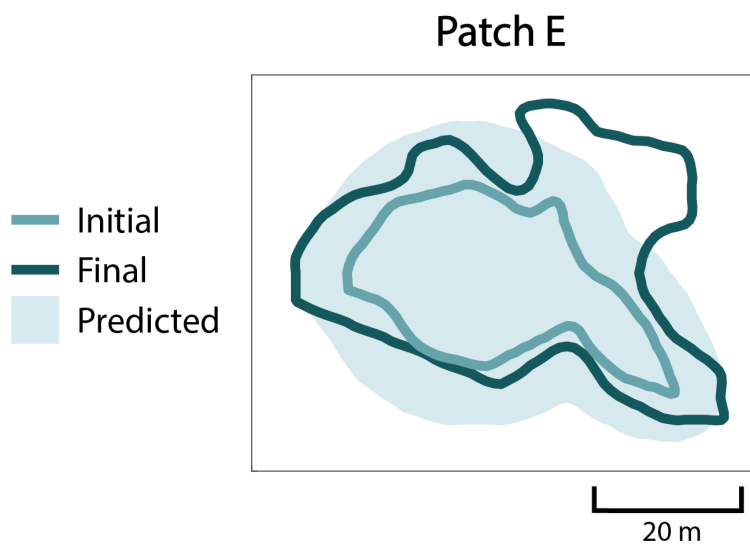


Figure E.5: Composite score of 0.833

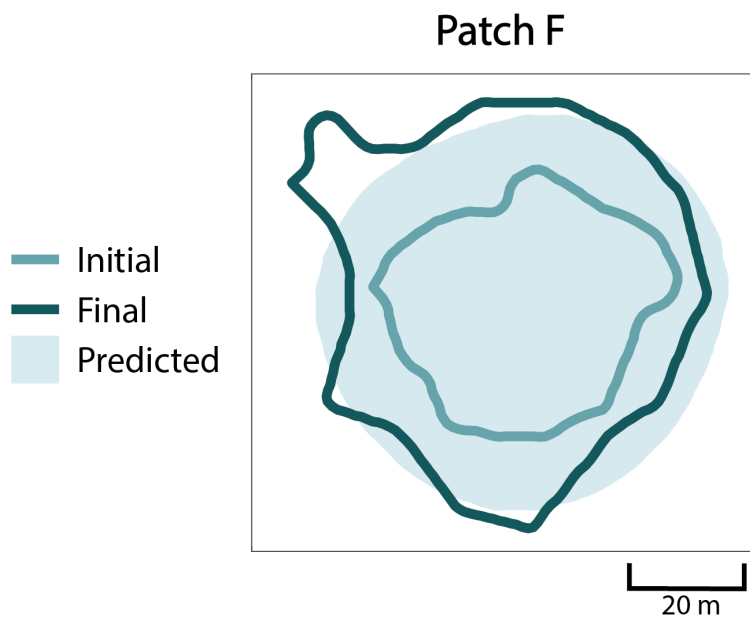


Figure E.6: Composite score of 0.796

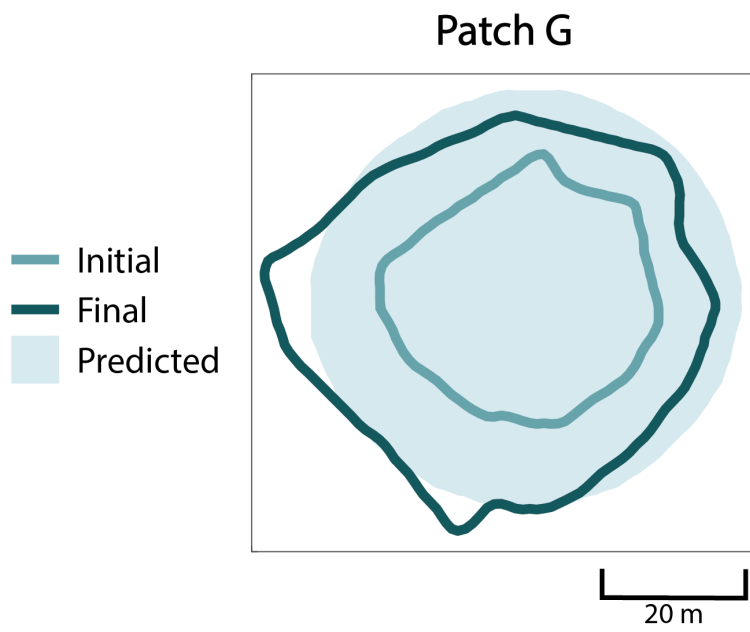


Figure E.7: Composite score of 0.880

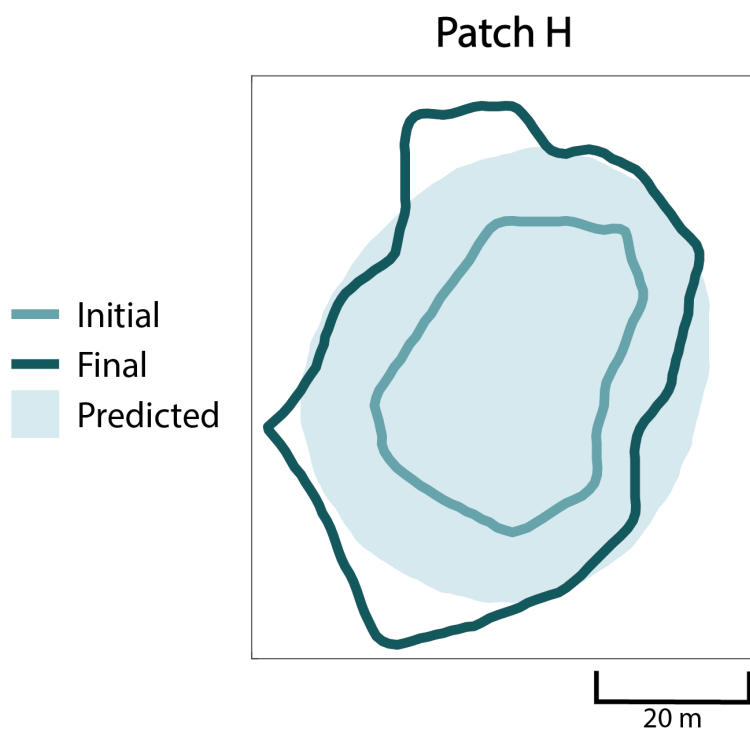


Figure E.8: Composite score of 0.818

## F All Spain Patch Predictions

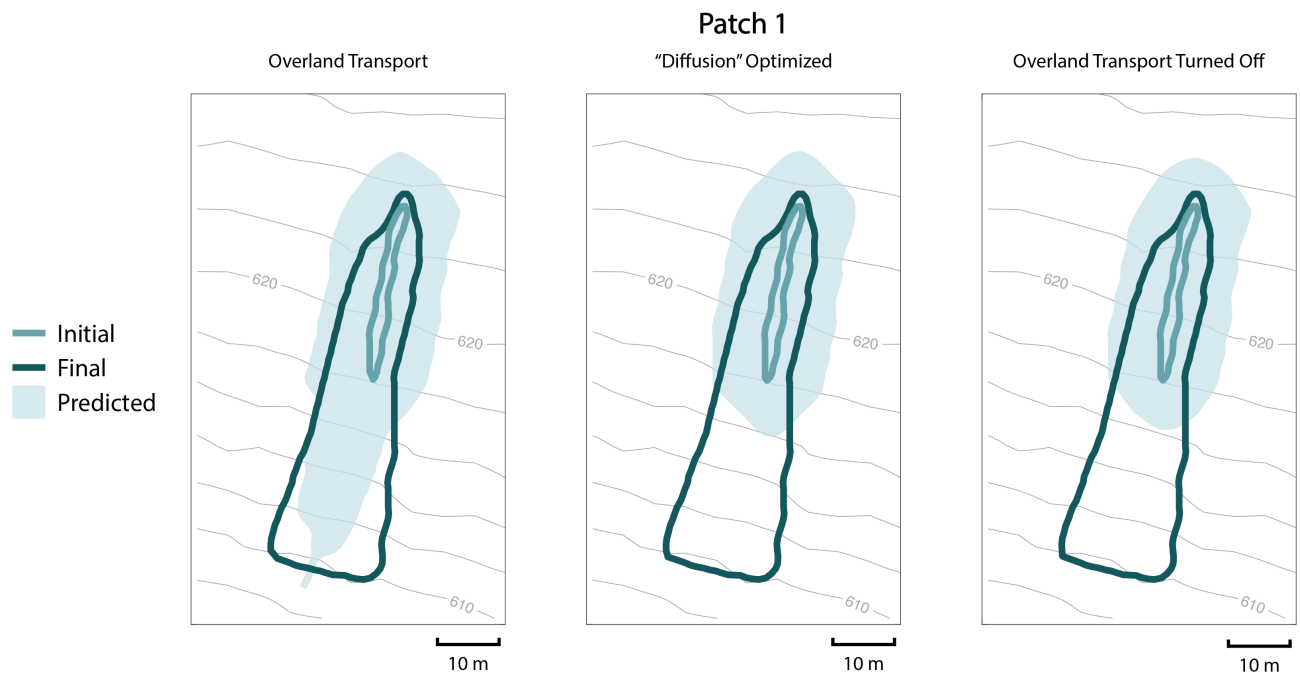


Figure F.1: Overland composite score of 0.866 ( $\alpha=0.085$ ), "diffusion" optimized composite score of 0.718, overland transport off composite score of 0.714

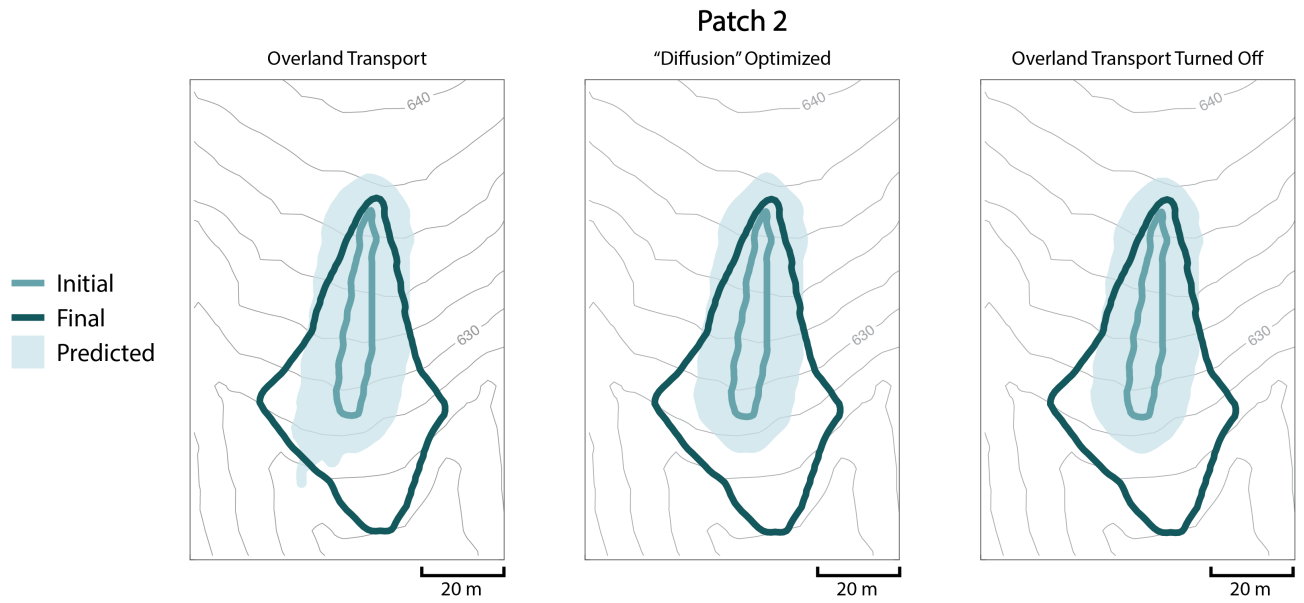


Figure F.2: Overland composite score of 0.833 ( $\alpha=0.110$ ), "diffusion" optimized composite score of 0.815, overland transport off composite score of 0.811

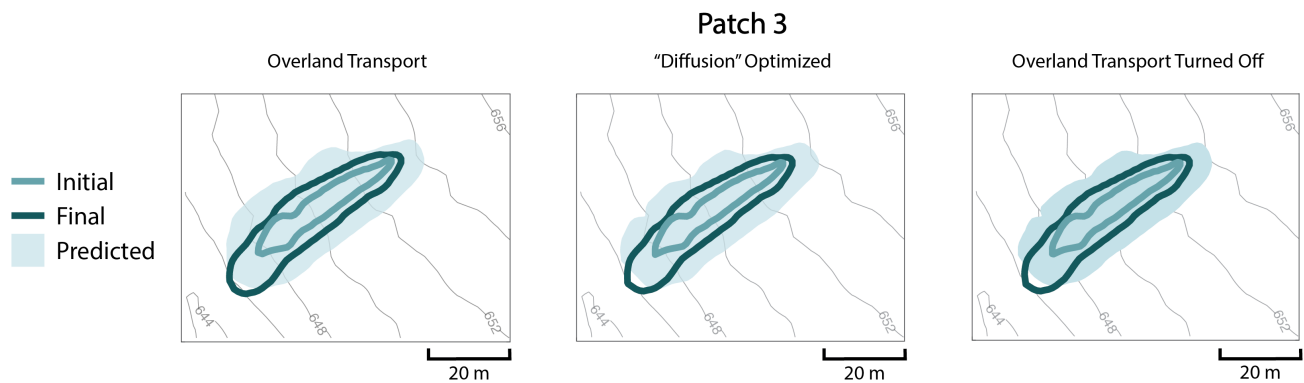


Figure F.3: Overland composite score of 0.834 ( $\alpha=0.285$ ), "diffusion" optimized composite score of 0.830, overland transport off composite score of 0.835



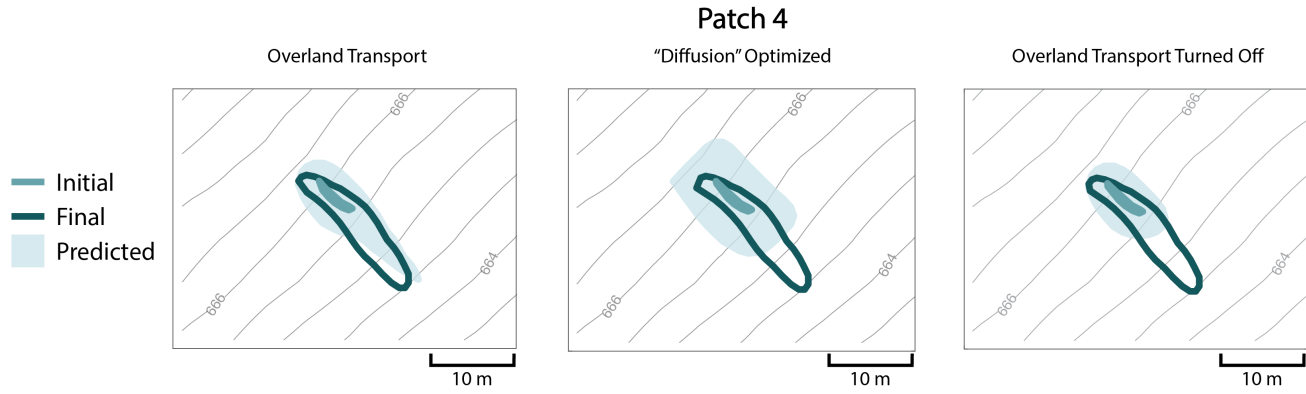


Figure F.4: Overland composite score of 0.860 ( $\alpha=0.025$ ), “diffusion” optimized composite score of 0.706, overland transport off composite score of 0.686

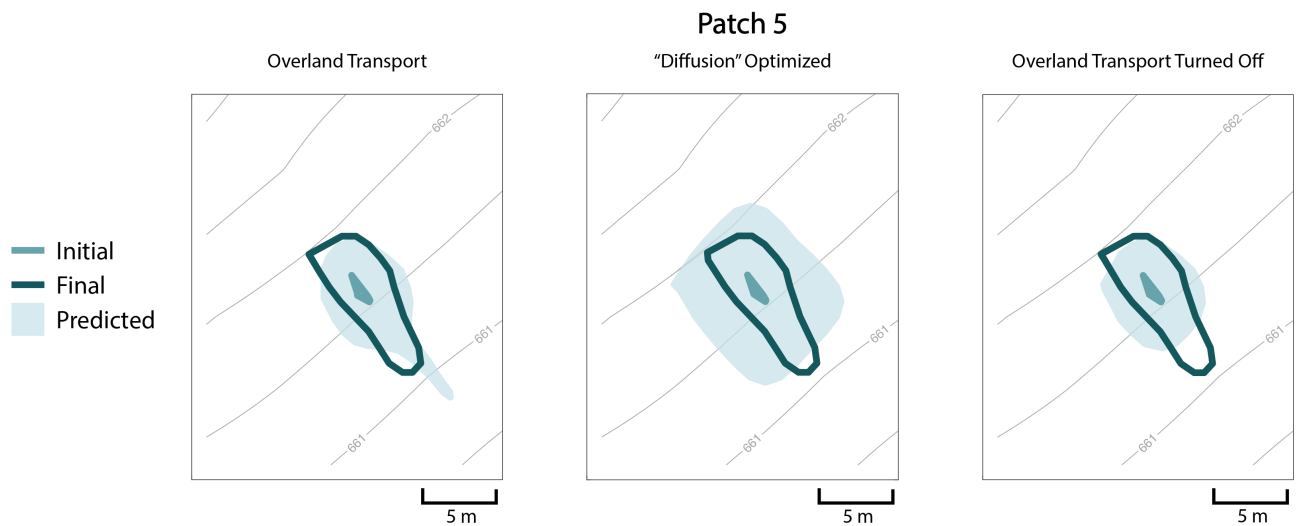


Figure F.5: Overland composite score of 0.885 ( $\alpha=0.015$ ), “diffusion” optimized composite score of 0.734, overland transport off composite score of 0.703

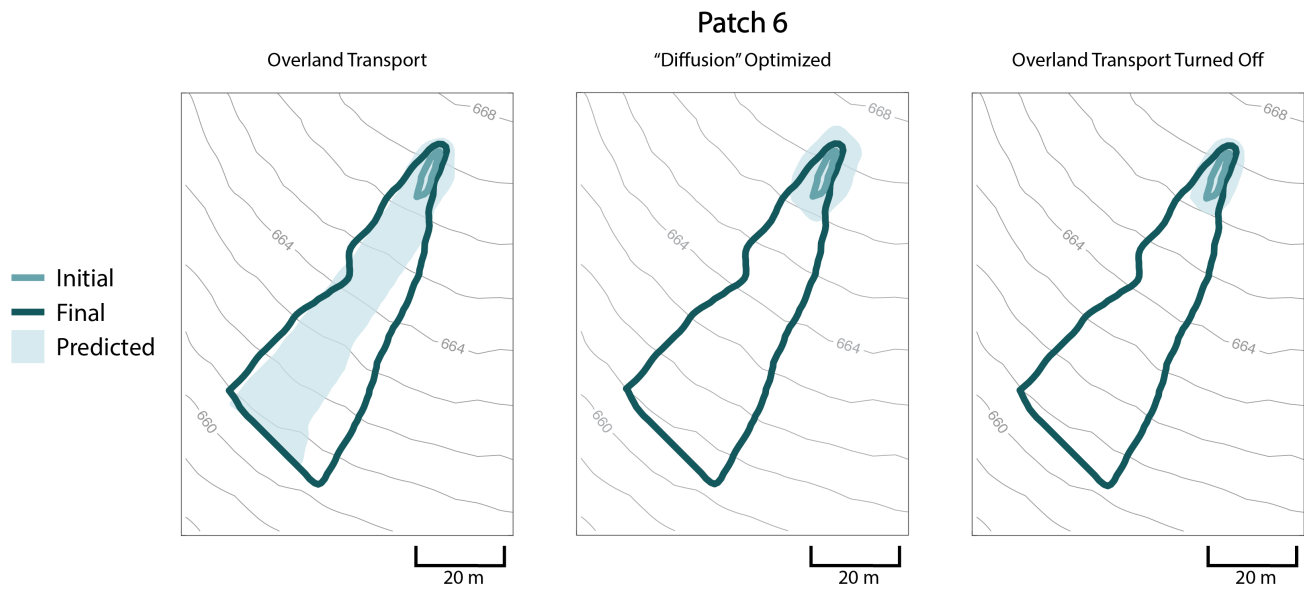


Figure F.6: Overland composite score of 0.859 ( $\alpha=0.007$ ), "diffusion" optimized composite score of 0.546, overland transport off composite score of 0.533

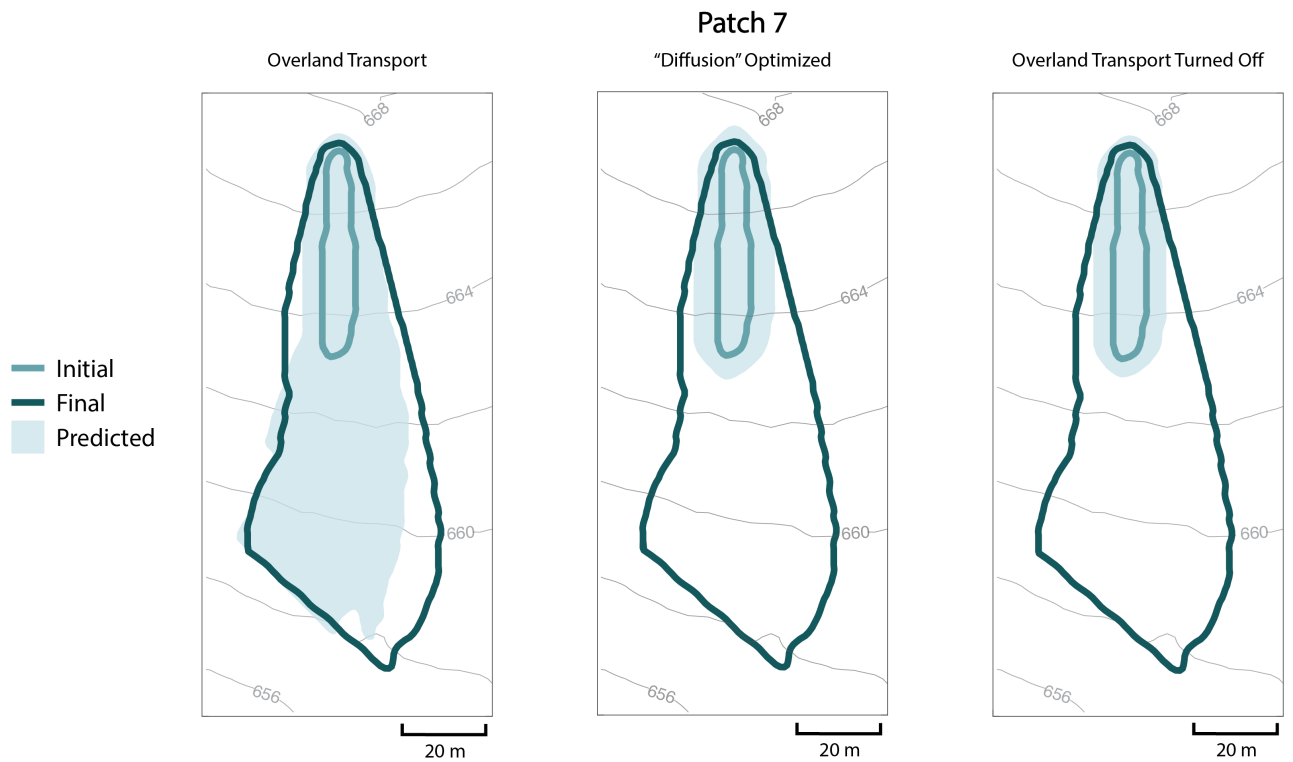


Figure F.7: Overland composite score of 0.913 ( $\alpha=0.0017$ ), "diffusion" optimized composite score of 0.658, overland transport off composite score of 0.646

## G Parameterization Results

Site	Configuration	$d$	$\Delta r$	$D_{max}$
Western Australia	Overland Transport	0.14	0.03	0.025
Spain	Overland Transport	0.12	0.04	0.0014
Spain	“Diffusion” Optimized	0.08	0.06	$7.5e^{-9}$

Table G.1: Tuned values for pathogen mortality rate ( $d$ ), pathogen growth rate temperature dependence ( $\Delta r$ ), and maximum pathogen diffusion coefficient ( $D_{max}$ ) for different tested configurations at both sites.

Patch	$\alpha$
1	0.085
2	0.110
3	0.285
4	0.025
5	0.015
6	0.007
7	0.0017

Table G.2: Tuned  $\alpha$  values specific to each patch at the Spanish site in the overland transport configuration.

## H Soil moisture dynamics

Histograms of the modeled soil moisture values for both sites are shown below. At the site in Western Australia, saturated conditions never occurred whereas at the Spanish site there were incidences of saturation ( $s = 1$ ) and therefore generation of overland flow, although these events were infrequent.

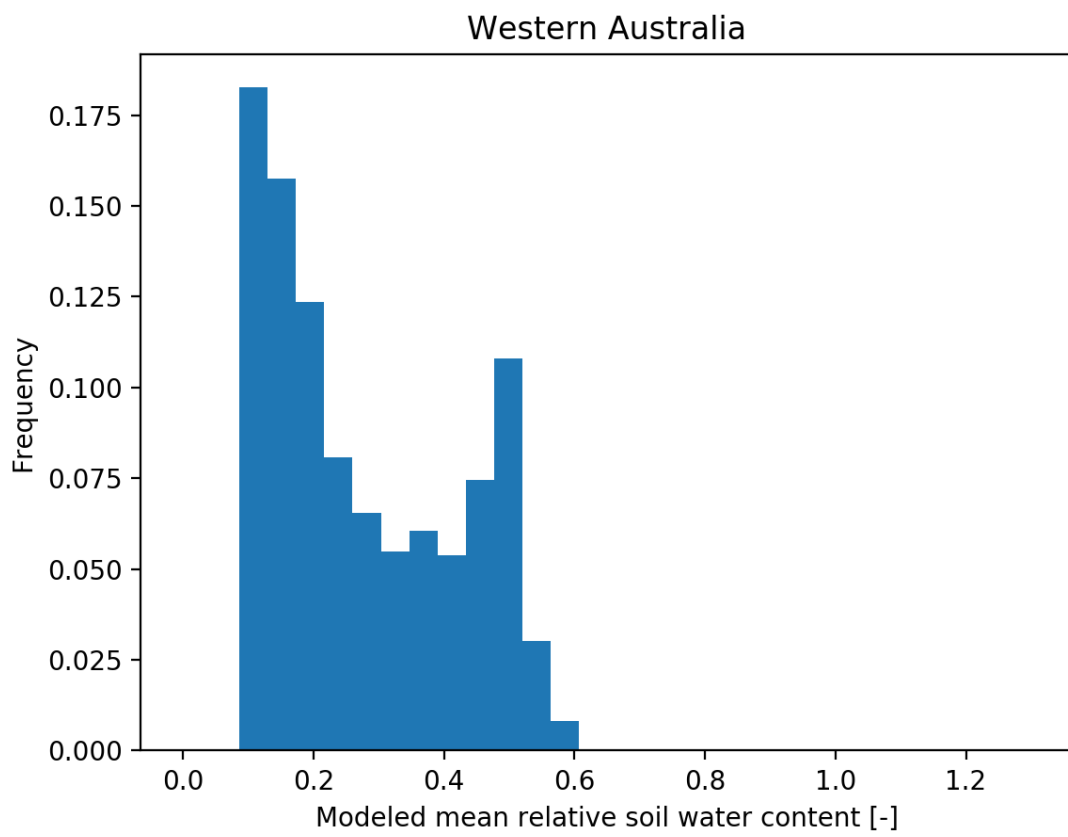


Figure H.1: Modeled soil moisture in Western Australia during the studied period

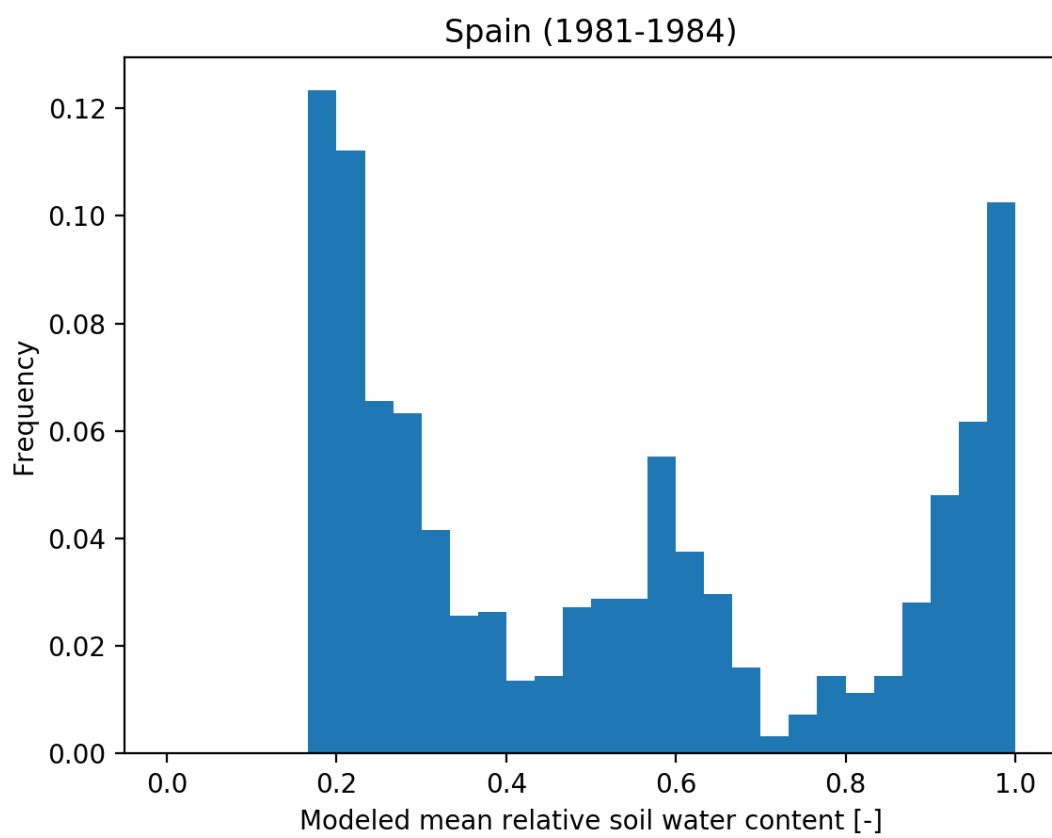


Figure H.2: Modeled soil moisture in Spain during the first studied interval between 1981-1984

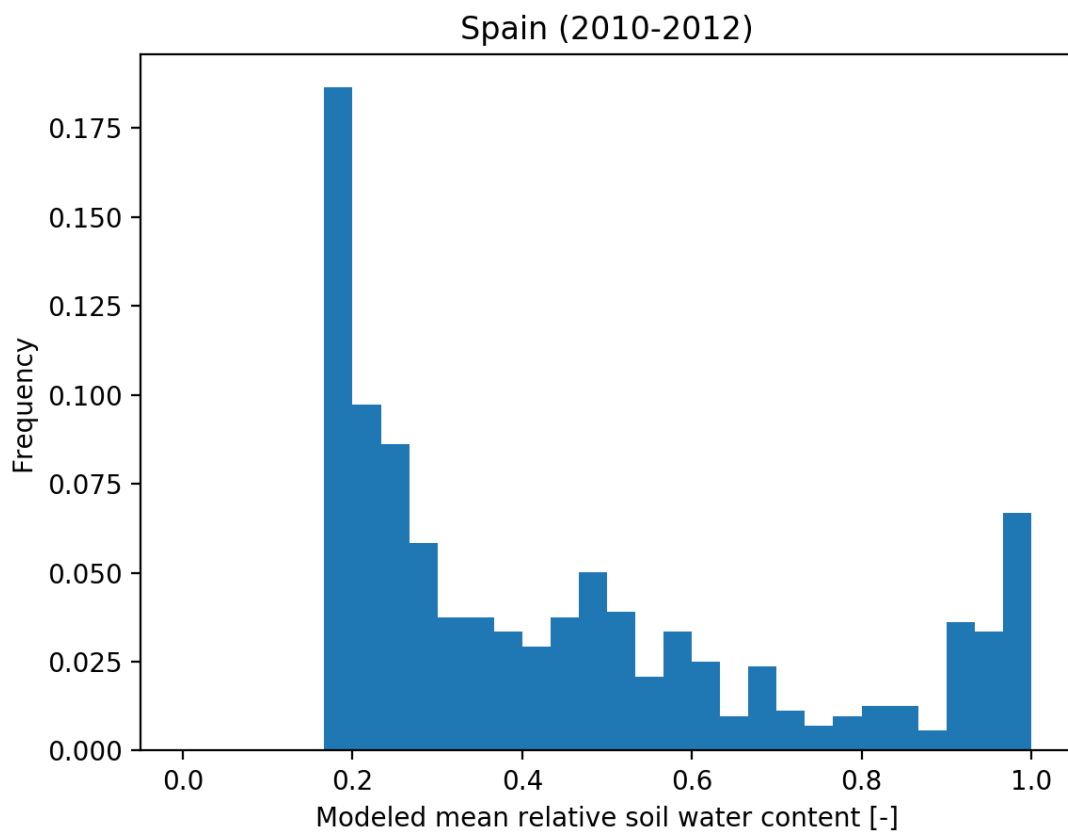


Figure H.3: Modeled soil moisture in Spain during the second studied interval between 2010-2012